PEOPLE'S DEMOCRATIC REPUBLIC OF ALGERIA

Ministry of Higher Education and Scientific Research

N° Série : ……/2022

University of Kasdi Merbah Ouargla

Faculty of Hydrocarbons, Renewable Energies and Earth and Universe Science

Hydrocarbon Production Department

Memory

To obtain the Master's Degree

Option: Academic Production

Presented by:

Messeguem Tarek, Refice Abdessalam, Salka Mohammed Chemseddine

-TOPIC-

NUMERICAL STUDY OF NON-NEWTONIAN FLUID FLOW THROUGH THE ANNULUS BETWEEN TWO CIRCULAR CYLINDERS, APPLICATION TO DRILLING MUDS AND/OR CRUDE OIL

Supported on: 08/06/ 2022 In front of the jury:

President:	Mr. BOUCHIREB ouahab	MCB	Univ.Ouargla
Reporter:	Mr. OUZZAZI mohamed	MAA	Univ.Ouargla
	Mr. BENAMOR ahmed	PhD Student	Univ.Ouargla
Examiner:	Mr. TOUAHRI abdeldjebar	MCB	Univ.Ouargla
Invited:	Mr. NECIB hichem	MAA	Univ.Ouargla
	Mm. BELMILOUD fatima zohra	MAA	Univ.Ouargla

Year: 2021/2022

Thanks

*We first thank **ALLAH**, the almighty who enlightened our way and gave us the courage, strength and patience to complete this work.*

*We would also like to thank our promoter **Mrs Ouzzazi Mohamed and Benamor Ahmed** for having accepted to lead this work with a lot of patience, we thank you for your guidance and advice that you gave us during this work.*

Thanks also go to the president of the jury and to the reviewers for doing us the honor of judging this work. We thank all those who contributed directly or indirectly to the achievement this brief. Finally, our thanks go to all teachers encountered in our course.

Tarek & Chemseddine & Abdessalam

DEDICATION

We dedicate this work to our parents for their love, patience, care, and continuous support during the five years of our study at the university.

To our wonderful parents who have raised us to be what we are, today. Thank you for everything.

To our brothers and sisters for their encouragement and love.

To all our family. To all our teachers. To our friends and colleagues without exception. We would like to say '' Thank you So much.

Abstract:

Drilling fluids play a key role in the well drilling operation. They are essential in maintaining pressure balance inside the wellbore**.**

One of the most influential properties of a drilling fluid is its viscosity. Understanding the role of viscosity in drilling and other operations and the ability to match viscosity requirements to prevailing conditions for that requirement is a key factor in optimizing fluid efficiency. the term rheology, which defined as the study of the deformation and flow of matter.

The Finite Volume Method (FVM) is a numerical technique that transforms the partial differential equations representing conservation laws over differential volumes into discrete algebraic equations over finite volumes (or elements, cells or meshes).

Computational fluid dynamics (CFD) analysis was performed to investigate the hydraulics of a solid-free non-Newtonian drilling fluid with an eccentric annulus coupled with a rotating drill string.

Keywords: Drilling fluids; Rheology; Herschel–Bulkley; Pressure drop; laminar flow; CFD analysis; flow-loop; eccentric annulus.

ملخص :

تلعب سوائل الحفر دورً اساسي في عملية حفر الآبار.والتي تعد ضرورية في الحفاظ على توازن الضغط داخل حفرة البئر.

تعد اللزوجة واحدة من أكثر الخصائص تأثيرًا لسائل الحفر. يعد فهم دور اللزوجة في الحفر عاملاً رئيسيًا في تحسين كفاءة السوائل.يمكن ان نعرف مصطلح الريولوجيا بأنه دراسة تشوه المادة وتدفقها.

طريقة الحجم المحدود (FVM) هي تقنية عددية تحول المعادلات التفاضلية الي معادلات جبرية.

تم إجراء تحليل رقمي لديناميكا الموائع (CFD) للتحقق من الخصائص الهيدروليكية لسائل الحفر الغير نيوتوني خالٍ من المواد الصلبة.

كلمات مفتاحية: سائل الحفر,الريولوجيا,تحليل رقمي,انخفاض الضغط.

Résumé :

Les fluides de forage jouent un rôle important dans le forage de puits. Ils sont essentiels pour maintenir l'équilibre de la pression à l'intérieur du puits de forage.

L'une des propriétés les plus influentes d'un fluide de forage est sa viscosité. Comprendre le rôle de la viscosité dans le forage et d'autres opérations permettre de l’optimisation de l'efficacité des fluids de forage. le terme rhéologie, défini comme l'étude de la déformation et de l'écoulement de la matière.

La méthode des volumes finis (FVM) est une technique numérique qui transforme les équations différentielles partielles aux équitions algébriques.

Une analyse de la dynamique des fluides computationnelle (CFD) a été réalisée pour étudier l'hydraulique d'un fluide de forage non newtonien sans solide avec la rotation de train de tige.

Mots clés : fluide de forage, simulation numérique, écoulement laminaire, pertes de charge, rhéologie.

Table of Contents:

List of Figures:

CHAPTER I: DRILLING FLUIDS

CHAPTER II: RHEOLOGY

CHAPTER III: THE FINITE VOLUME METHOD

CHAPTER IV : CFD ANALYSIS

List of Tables:

CHAPTER I: DRILLING FLUID

CHAPTER II: RHEOLOGY

CHAPTER III: THE FINITE VOLUME METHOD

CHAPTER IV: CFD ANALYSIS

List of Symbols:

Term	Symbol (s)	Unit(s)
Eccentricity	e	-
Equivalent circulating density	ECD	lb/gal SG Kg/m^3
Friction factor	f	-
Effective viscosity	-	Cp or Pa.sec
Flow index	n	-
Consistency index	K	Cp.Pa sec^n $lb/100\ ft^2sec^n$
Plastic viscosity	PV Or µp	Cp or Pa.sec
Pressure drop	-	Pa/m

Reynolds Number	Re	-
Shear Rate	$\dot{\gamma}$	$1/s$
Fluid Viscosity	μ	cp

General Introduction

A major component in drilling operation success is drilling fluid performance.Drilling fluids are classified into three categories, these three major categories include Pneumatic, Oil-Based mud **(OBM)** and Water-Based mud **(WBM)** fluids.

The key objective to learning is to understand some principles of hydraulics and wellbore pressure management

The Finite Volume Method (FVM) is a numerical technique that transforms the partial differential equations representing conservation laws over differential volumes into discrete algebraic equations over finite volumes (or elements, cells or meshes).

Computational fluid dynamics (CFD) analysis was performed to investigate the hydraulics of a solid-free non-Newtonian drilling fluid with an eccentric annulus coupled with a rotating drill string.

Problems:

Lost circulation from the formation into the wellbore might occur if the pressure inside the wellbore is not controlled. Apart from maintaining wellbore pressure, drilling fluids play a major role in transporting cuttings to the surface.

An appropriate cuttings transport avoids many problems, such as stuck pipe, slow rate of penetration (ROP), formation fracturing, premature bit wear, or high torque and drag on the drill string.

Proper estimation of the frictional pressure loss is also important in drilling operations. Poor estimation of the frictional pressure loss might lead to serious problems in the determination of hydraulic power requirements of pumps.

CHAPTER

I

Drilling fluids

I.1 Introduction

Drilling fluids (muds) are complex heterogeneous fluids, consisting of several additives that were employed in drilling of oil and natural gas wells since the early 1900. The original use of the drilling fluids was to remove cuttings continuously. Progress in drilling engineering demanded more sophistication from the drilling mud. In order to enhance the usage of drilling fluids, numerous additives were introduced and a simple fluid became a complicated mixture of liquids, solids and chemicals as the drilling fluids evolved, their design changed to have common characteristic features that aid in safe, economic and satisfactory completion of a well. (1)

The drilling fluid is related either directly or indirectly to almost every drilling problem. This is not to say that the drilling fluid is the cause or solution of all drilling problems, but it is a tool that can often be used to alleviate a problem situation.

Generally, a good drilling fluid is simple and contains a minimum number of additives. This allows easier maintenance and control of properties. It is desirable to have a mud system that is flexible enough to allow changes to be made to meet changing requirements as they occur.

Running a mud system consists primarily of controlling the type and amount of solids in the mud and their chemical environment. All mud properties are controlled by controlling these compositional factors. Accurate mud tests are necessary for proper control of the mud properties. (2)

I.2 Drilling Fluid Classifications

Drilling fluids are classified into three categories, these three major categories include Pneumatic, Oil-Based mud **(OBM)** and Water-Based mud **(WBM)** fluids. Each has many subcategories based on purpose, additives, or clay states **(See Figure I. 1)**.

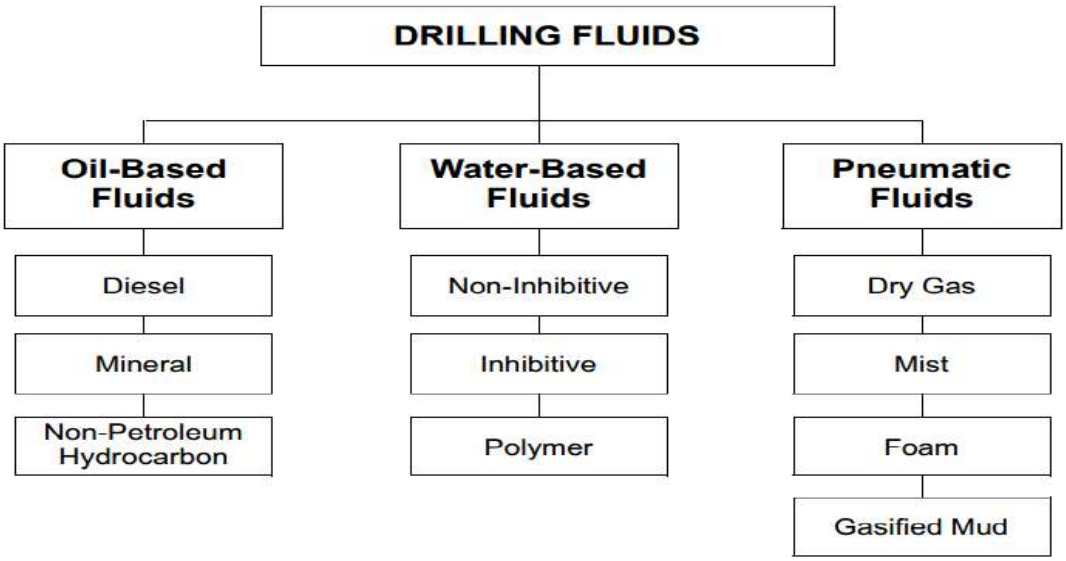

Figure I. 2- Drilling fluids classification (3)

I.2.1 Pneumatic Fluids

Pneumatic drilling fluids are recommended for formation where there is potential for circulation loss. Pneumatic drilling fluids are used for underbalanced drilling. Pneumatic drilling is known to have improved rate of penetration, better control of loss circulation zones and less damage to formations. However, Pneumatic drilling fluids especially dry air/natural gas, have been responsible for causing fire and corrosion to down-hole equipment. (1)

Foams: Mixture of air, water and detergent foaming agent. (4)

I.2.2 Oil-Based Fluids

Oil based fluids use crude or refined oils as the continuous phase. These muds may have water emulsified in the oil. Two types of oil-based fluids are commonly used. An oil mud has less than 5% water. An invert emulsion has a water concentration greater than 5%.

- The oil base fluids are generally used for specific purposes.

- Such as drilling sensitive production zones or problem shales.
- Drilling salt section and formation that contain hydrogen sulfide.
- Danger of stuck pipe problems, and drilling at bottom hole temperatures that are permissible by water base muds.
- Low-gravity solids content has to be monitored closely when drilling with oil base muds since at this environment solids do not hydrate which causes low-gravity solids contents to exceed acceptable levels often. This results in reduction of penetration rate, formation damage and increase in risk of differential sticking.

Since oil-base muds contain substantially less colloidal particles, they exhibit a spurt fluid loss. Due to the higher filtration rates, the monitoring of high-pressure high-temperature filtration as well as the drilling conditions are important to ensure that excessive filtration or filter cake buildup does not lead to problems. (5)

I.2.3 Water-Based Fluids

Water based fluids are the most extensively used drilling fluids. They are generally easy to build, inexpensive to maintain, and can be formulated to overcome most drilling problems. In order to better understand the broad spectrum of water-based fluids, they are divided into three major sub classifications **(See figure I. 3)**:

- Inhibitive
- Non-inhibitive
- Polymer

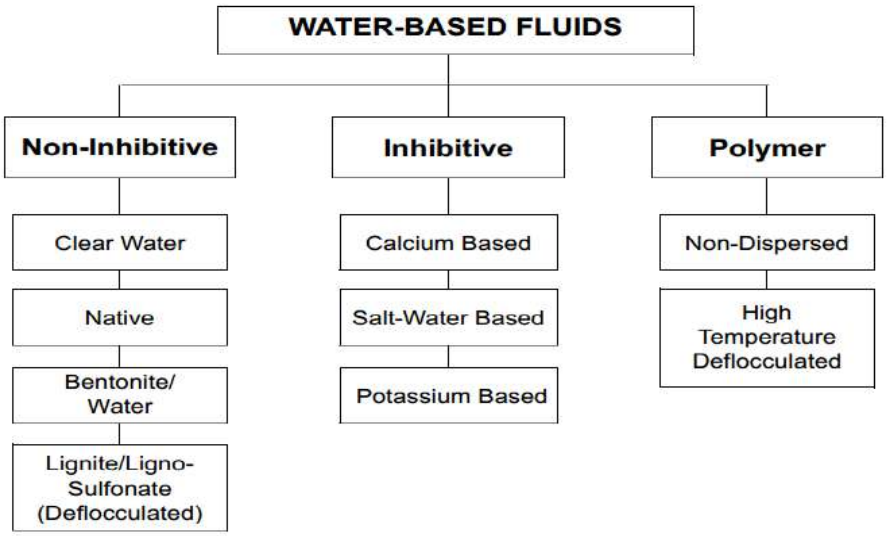

Figure I. 4-Water based fluids. (3)

I.2.3.1 Non-Inhibitive Fluids

Those which do not significantly suppress clay swelling, are generally comprised of native clays or commercial bentonites with some caustic soda or lime. Non-inhibitive fluids are generally used as spud muds. Native solids are allowed to disperse into the system until rheological properties can no longer be controlled by water dilution.

I.2.3.2 Inhibitive Fluids

Those which appreciably retard clay swelling and, achieve inhibition through the presence of cations; typically, Sodium (Na^+), Calcium (Ca^{++}) and Potassium (K^+). Generally, K^+ or Ca^{++}, or a combination of the two, provide the greatest inhibition to clay dispersion. These systems are generally used for drilling hydratable clays and sands containing hydratable clays.

I.2.3.3 Polymer Fluids

Those which rely on macromolecules, either with or without clay interactions to provide mud properties, and are very diversified in their application. These fluids can be inhibitive or non-inhibitive depending upon whether an inhibitive cation is used.

Polymers can be used to viscosify fluids, control filtration properties, deflocculate solids, or encapsulate solids. The thermal stability of polymer systems can range upwards to 400°F. In spite of their diversity, polymer fluids have limitations. Solids are amajor threat to successfully running a cost-effective polymer mud system. (3)

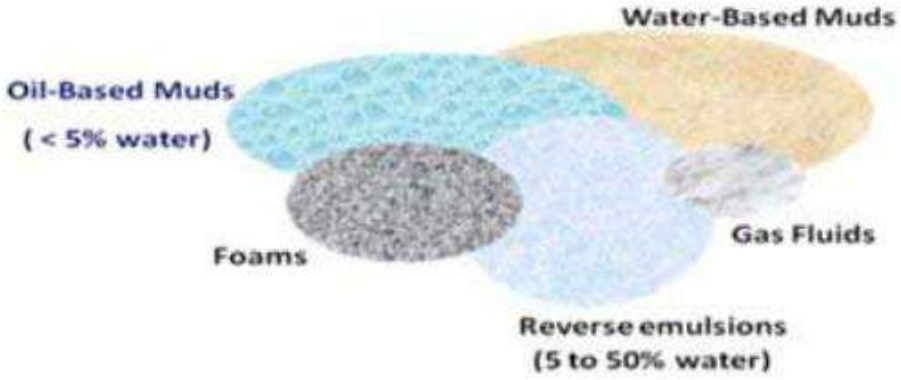

Figure I. 5-Drilling fluid types. (6)

I.3 Clay chemistry

Thus, an understanding of clay chemistry is important in the selection of a drilling fluid system and borehole stability. Most reservoir sandstones also contain some clay minerals. These may react with the fluids that contact the min such a way as to completely block the formation.

Therefore, the structures and reactions of clays are important in the design of fluids that may be in contact with the producing zone. Clays play a significant role in drilling fluids, particularly in water base fluids.

They may be added intentionally to control the viscous flow properties and to provide the colloidal properties required for filtrate loss control, or they may build up through drilling of formations in which they predominate. Commercial clays such as bentonite and attapulgite are purposely added to enhance drilling fluid properties.

However, since the combination of formation clays and commercial clays frequently leads to too much viscosity, a large group of chemicals, including those

described as “mud conditioning chemicals”, are added to control the viscous properties. (7)

I.4 Drilling Fluid Circulation System

Dyke (2003) presented in his book the drilling fluid circulation systems with the different equipment (mud tank, mud pumps, mud pits, mud-mixing equipment and contaminant removal equipment) that the drilling mud passes through it as shown in figure 4.

First, drilling mud is stored in mud tanks existed near the rig then, mud pumps force the drilling mud at high pressure to the pump manifold which located at the derrick floor. From the manifold, the mud reaches the rig within the standpipe, after that, the mud passes in the drill string through swivel (permits rotating the drill string while the fluid is pumped down) which present at the top of the Kelly.

Then, the drilling mud passes down through the rotating drillstring to the drill bit at the bottom of the hole. The drilling mud then travels up to the surface through the annular space between the borehole wall and rotating drillstring and finally to the suction mud tank through the shale shaker (separate the cuttings from the drilling mud) **(See figure I. 6).** (8)

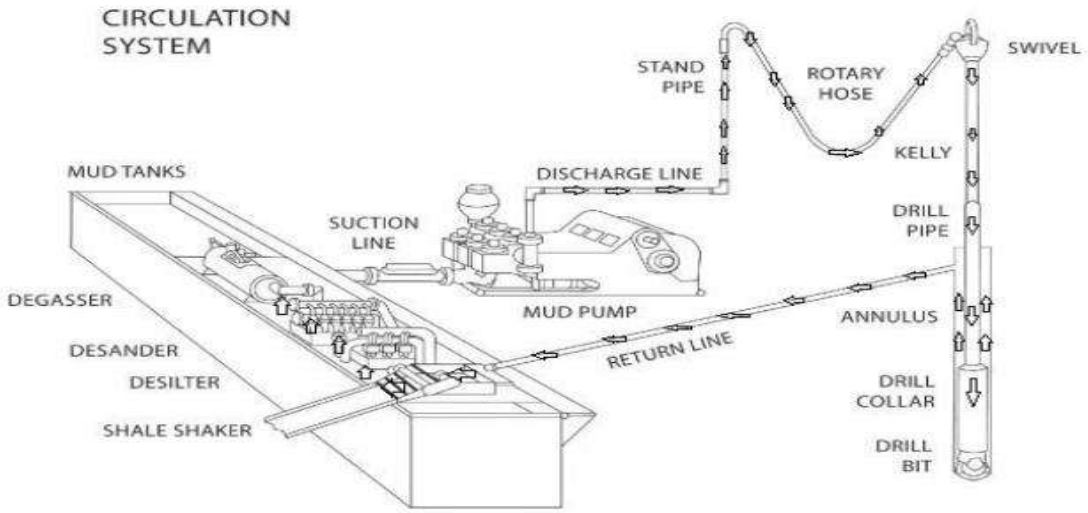

Figure I. 7-Drilling mud circulation system. (8)

I.5 Functions of Drilling Fluids

I.5.1 Major Functions

Drilling fluids are designed and formulated to perform three major functions:

- Control Subsurface Pressure.
- Transport Cuttings.
- Support and Stabilize the Wellbore.

I.5.1.1 Control Subsurface Pressure

A drilling fluid controls the subsurface pressure by its hydrostatic pressure. Hydrostatic pressure is the force exerted by a fluid column and depends on the mud density and true vertical depth (TVD). (3)

I.5.1.2 Transport Cuttings

Fluid flowing from the bit nozzles exerts a jetting action to clear cuttings from the bottom of the hole and the bit, and carries these cuttings to the surface. Several factors influence cuttings transport. (3)

I.5.1.3 Support and Stabilize Wellbore

Fluid hydrostatic pressure acts as a confining force on the wellbore. This confining force acting across a filter cake will assist in physically stabilizing a formation.

Borehole stability is also maintained or enhanced by controlling the loss of filtrate to permeable formations and by careful control of the chemical composition of the drilling fluid. (3)

I.5.2 Minor Functions

Minor functions of a drilling fluid include:

- Support Weight of Tubulars.
- Cool and Lubricate the Bit and Drill String.

- Transmit Hydraulic Horsepower to Bit.
- Provide Medium for Wireline Logging.

I.5.3 Additional Benefits

In addition to the essential functions of a drilling fluid, there are other benefits to be gained from proper selection and control, such as to:

- Minimize Formation Damage.
- Reduce Corrosion.
- Minimize Lost Circulation.
- Reduce Stuck Pipe.
- Reduce Pressure Losses.
- Improve Penetration Rates.
- Reduce Environmental Impact.
- Improve Safety. (3)

I.6 Selection of a Drilling Fluid

Bleier (1990) emphasized that the selection of the appropriate drilling mud is paramount to the success of a drilling process. Many choices are available with different drilling fluid types, different base fluids, different chemical additives and different physical properties. Drilling mud selection depends on numerous factors such as safety, high temperatures and pressures, shale problems, salt problems, environmental considerations and economics as shown in table 1. (8)

I.6.1 Safety issues

The fluid must be able to provide the mud density required to control the well. Speed and ease with which a mud will accept weighting materials can be important in kick situations.

Many mud types are uncapable to control well especially when mud weights exceed 15 Ibm/gal. So, polymer muds will need some dispersant and oil muds will need oil/water ratios higher than 50/50. In deep-water drilling, gas hydrates can overlap mechanically with well-control conditions.

Water-based muds especially salt muds are currently the favorable fluids of choice in deep water due to its high salinity which suppresses the hydrate formation. The safest muds for drilling zones bearing H_2S should contain at least 10 Ibm/bbl excess limeplus a sulfide scavenger. Oil and lime drilling muds are the only two mud types that are compatible with this case. (8)

I.6.2 High Temperatures and Pressures

At high downhole temperatures and pressures, fluid loss problems occur for most water-based fluids, but fluid loss are controlled by using oil-based muds. So, oil fluids are a viable at these high temperatures and pressures. (8)

I.6.3 Shale problems

Shale formations can disperse, slough or swell into the hole. Shale swelling are the most common mud-related drilling problem occur around the world. This type of problem is mechanical in nature. Increasing the mud density and the appropriate composition of drilling muds are important to the solution. Theory and experience indicate that asphaltic agents reduce sloughing, long chains polymers reduce dispersion, and dissolved salts reduce swelling.

Laboratory tests showed that water-based muds are unsuccessful in eliminating shale problems due to its high dissolved salts which cause shale swelling. But, oil-based muds eliminate shale problems because they provided adequate mud weight and enough salinity of the aqueous internal phase. (8)

I.6.4 Salt Problems

Salt formations are unique. Salt has little porosity and permeability. It can flow plastically through other geological rock beds under stress with "salt creep" resulting in wellbore size reduction and casing collapse. Salt can also dissolve in water necessitating the salinity of a water-based fluid be kept near or at saturation to avoid or minimize wellbore enlargement that can lead to poor cementing of the casing and deficient zonal isolation. (8)

I.6.5 Environmental considerations

Environmental considerations that related to the process of drilling mud are varied depending primarily on the well location. Many restrictions present to the avoidance of using oil fluid in some locations, salt muds in other locations, chromium-treated muds in still other locations. Drilling-fluid bioassay tests are useful for assessing the toxicity of special additives. So, the search for alternative materials instead of some original toxicity additives continues to be the highest research priority in drilling fluids. (8)

I.6.6 Economics

It includes the cost of the base fluid and the additives, maintenance costs, mud-related disposal costs, type of drilling either underbalanced or overbalanced total costs and for oil muds, buy-back provisions. In some regions, the waste management can represent a high percentage of the total well cost **(See Table below).**

The most critical part is the volume resulting from dilution. Many companies do not require expensive muds in some wells which make them use some types of low-cost muds such as lignite muds, native-brine starch muds, unweighted-gel freshwater muds muds, but in some cases the using of synthetic oil-based mud becomes more cost effective that makes the industry to use the WBM (8)

Table I. 1- selection of drilling mud. (8)

	Water based mud	Oil based mud
Safety issues	Low	High
HPHT	High	Low
Shale problems	High	Low
Salt problems	High	Low
Environmental consideration	Low	High
Economics (cost)	Low	High

I.7 Drilling Mud Properties

In order to gain better control over the mud system, a more meaningful monitoring strategy of the mud properties is important. The mud program is not the same for every well. In fact, in the course of drilling a well, the composition of the mud can be changed in order to deal with variations in the formation properties and mechanical factors that affect the drilling rate. (9)

I.7.1 Density or mud weight

The starting point of pressure control is the control of mud density. The weight of a column of mud in the hole necessary to balance formation pressure is the reference point from which all pressure control calculations are based. The required weight of

The mud column establishes the density of the mud for any specific case. Fortunately, density is one of our most accurate measurements. With a simple mud balance **(See figure below)**, we are able to weigh a mud to the nearest 0.1 lb. / gal, which is equivalent to 5.2 psi per 1000 ft. of mud column. (7)

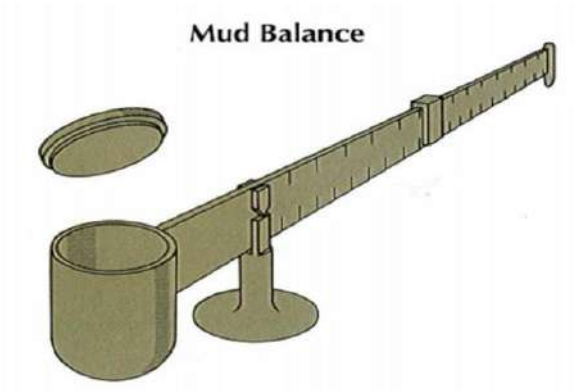

Figure I. 8-Baroid mud balance (2)

I.7.2 Fluid loss (Filtration)

It is generally defined as the volume of the drilling mud that passes into the formation through the filter cake formed during drilling. It is often minimized or prevented by blending the mud with additives. A number of factors affect the fluid-loss

properties of a drilling fluid, including time, temperature, cake compressibility; but also, the nature, amount and size of solids present in the drilling fluid. (6)

I.7.3 Solids, Oil, And Water Content

Solids, Oil, And Water Content are measured not only as a basis for the control of the oil content of emulsion muds, but also as an aid in the control of the performance of the mud. Solids content affects drilling rate and flow properties of the mud. Optimum solids control is essential for overall superior mud performance. (4)

I.7.4 Drilling Fluid PH

The measure of the hydrogen ion concentration in a solution which indicates the alkalinity or acidity of fluid. Two methods for measuring the pH of drilling fluid are commonly used:

- A modified colorimetric method using pH paper or strips.
- The electrometric method using a glass electrode.

The paper strip test may not be reliable if the salt concentration of the sample is high. The electrometric method **(See figure below)** is subject to error in solutions containing high concentrations of sodium ions unless a special glass electrode is used or unless suitable correction factors are applied if an ordinary electrode is used. In addition, a temperature correction is required for the electrometric method of measuring Ph. (10)

Figure I. 9- The ph metre (5)

I.7.5 Sand Content

Sand Content is measured because sand is abrasive to the equipment that comes in contact with the mud and sand may cause trouble by setting in the hole or by increasing the mud weight. (4)

I.7.6 Chemical Properties

The chemical properties of drilling fluids are central to their performance and the stability of wellbore. Thus, well properties that must be anticipated include the dispersion of formation clays and dissolution of salt formations.

This is because certain mud additives like polymers are affected by pH, $Ca^{2+}$and corrosion, which might be caused by dissolution of salty clay formations.

Therefore, rig side measurements should rely on simple chemical analyses to determine pH, Ca^{2+}, total hardness, concentration of Cl^{-} and sometimes K^{+}. The dispersion of clay in a water-based system, and observed that specific cations such as K^{+} and Ca^{2+} inhibited water sensitive formation from dispersing as the result of exchange of cations with the clay in the shale, thereby creating a more stable rock that is able to resist hydration.

The movement of water-based mud filtrate from the wellbore into the surrounding shale discovered that such movement is controlled by the difference between chemical potentials of the various species with the formation. The chemical potentials depend on the mud hydrostatic pressure in the wellbore and on its chemical composition. (9)

I.7.7 Resistivity

Control of the resistivity of the mud and mud filtrate while drilling may be desirable to permit enhanced evaluation of the formation characteristics from electric logs. The determination of resistivity is essentially the measurement of the resistance to electrical current flow through a known sample configuration.

Measured resistance is converted to resistivity by use of a cell constant. The cell constant is fixed by the configuration of the sample in the cell and id determined by

calibration with standard solutions of known resistivity. The resistivity is expressed in ohm-meters. (10)

I.7.8 Corrosivity

Corrosion has been found to be the principal cause of drill pipe failures. Corrosion of the surface of the drill pipe is monitored by placing steel rings in the tool-joint box recess at the end of the pin and determining the loss in weight after a selected time of exposure to the drilling fluid. Observation of the type of corrosive attack is frequently more significant than observation of the loss in weight.

In planning the drilling fluids program, attention must be given not only to the possible corrosive effects of the corrosion inhibitors on the drilling fluid itself.

Some corrosion inhibitors, for example, may severely affect the properties of water muds. Sources of corrosive agents, their composition, and methods of counteracting them are factors to be considered in selecting the drilling fluid. (5)

I.8 Drilling Mud Additives

Each drilling fluid vendor provides a wide array of basic and specialty chemicals to meet the needs of the drilling industry. The properties of drilling muds can be adjusted to meet any reasonable set of conditions, thereby overcoming most drilling problems such as abnormal pressures, lost circulation and sloughing shale. (9)

I.8.1 Viscosifiers (Filtrate Reducers)

Viscosifiers such as bentonite, CMC, Attapulgite clays, sub-bentonites, and asbestos fibers are employed in drilling fluids to ensure a high viscosity–solids ratio. (10)

I.8.2 Weighting Agents

These are materials added to increase the overall density of the drilling fluid so that sufficient bottom hole pressure can be maintained thereby preventing an unwanted

influx of formation fluids. Examples are barite, calcium carbonate, galena, lead sulphide and hematite. API barite, a dense inert mineral having a specific gravity near 4.2, can be added to any clay/water mixture to increase the density. (9)

I.8.3 Thinners (Deflocculants)

These chemicals modify the relationships between the viscosity and percentage of solids in a drilling mud, and may further be used to vary the gel strength, increase a mud's "pump ability," etc., Lignosulfonates, Tannins (quebracho), various polyphosphates and lignitic materials are chosen as thinners or as dispersants, since most of these chemicals also remove (by precipitation or sequestering, and deflocculation reactions) solids. Principle purpose of a thinner is to function as a deflocculant to combat random association of clay particles. (4)

I.8.4 Foaming agents

Foaming agents are most often chemicals that also act as surfactants (surface-active agents) to foam in the presence of water. These foamers permit air or gas drilling through water-production formations. (10)

I.8.5 Lost Circulation Materials

The primary function of lost circulation additives is to plug zone of loss back in the formation away from the face of the borehole so that subsequent operations will not result in a loss of drilling fluids. These materials include: hay, saw dust, bark, cotton seed hulls, laminated (flat) materials such as mica, cellophane, granular bridging materials such as nutshell, berlite and ground plastic. (9)

I.8.6 Flocculants

Flocculants are used sometimes to increase gel strength. Salt (or brine), hydrated lime, gypsum, and sodium tetraphosphates may be used to cause the colloidal particles of a suspension to group into bunches of “flocks,” causing solids to settle out. (10)

I.8.7 Lubricants

Lubricants are designed to reduce torque to increase horsepower at the bit by reducing the coefficient of friction. Certain oils, graphite powder, glycols and soaps are used for this purpose. (4)

I.8.8 Corrosion Inhibitors

Hydrated lime, aluminiumbisulphate, zinc chromate and amine salts are often added to muds to check corrosion. A good fluid containing adequate percentage of colloids, certain emulsion muds and oil muds should exhibit excellent corrosion inhibiting properties. (9)

I.8.9 PH Control Additives

PH control additives are products designed to control the degree of acidity or alkalinity of a drilling fluid. These additives include lime, caustic soda, and bicarbonate of soda. (10)

I.8.10 Bactericides

Bactericides reduce the bacteria count of a drilling fluid. Paraformaldehyde, caustic soda, lime, and starch are commonly used aspreservatives. (10)

I.8.11 Oxygen Scavenger

Commonly a sodium sulfite, ammonium bisulfite, frequently catalyzed with heavy metal such as nickel or cobalt. Oxygen scavengers react with dissolved oxygen in the water phase and remove it through this process. Oxygen scavenger should be injected into the line just before the pump, not into the suction pit. (4)

I.8.12 Hydrogen Sulfide Scavenger

Hydrogen Sulfide Scavenger - Usually a heavy metal (iron, zinc) chemical which, under proper conditions can chemically react with H_2S or neutralized sulfide species. Mud should have pH over 10 to protect steel components, then add the scavenger to react with and remove sulfide in an inert form. (4)

I.9 Conclusion

Drilling fluid -mud - is usually a mixture of water, clay, weighing material and a few chemicals. Sometimes oil may be used instead of water, or oil added to the Water to give the mud certain desirable properties. Drilling fluid is used to rise the cuttings made by the bit and lift them to the surface for disposal. But equally important, it also provides a means of keeping underground pressures in check. (11)

CHAPTER

II

Rheology

II. Chapter II

II.1 Introduction

In the oil and gas drilling industry, drilling fluids are very complex and are manufactured using certain additives in order to provide the required tribological and rheological properties for specific drilling methods and reservoir conditions. (12)

Drilling fluids are generally divided into water-based mud **(WBM)**, retarded WBM, oil-based mud **(OBM)**, synthetic-based mud **(SBM)**, foam, gas or air fluid, emulsion, etc.

WBM fluids are the fluid of choice for drilling due to their environmental properties and lower operating costs, but OBM is the fluid of choice for deep hole drilling and high-pressure high temperature **(HPHT)** drilling. This is partly attributed to the ionic nature of water molecules in WBM, where the positive charge on the hydrogen side attracts the negative charge on the oxygen side of the water molecule through van der Waals forces. Therefore, **WBM tends to generate higher internal friction compared to OBM.** (13)

Drilling fluids exhibit different flow behavior characteristics in the tubing, annulus, and bit nozzles during drilling operations. These features are sine qua non for efficient cuttings disposal and wellbore cleanup activities.

The phenomenon of abnormal flow behavior can cause serious operational problems, such as bridging in the wellbore, filling the bottom of the well with drill cuttings, reduction of penetration rate, wellbore enlargement, stuck tubing, etc , loss of circulation, kick and eventual blow out.

During drilling operations, it is important to correctly determine the hydrodynamic behavior of the well annulus drilling fluid within the "operating window" to maintain the correct pressure and avoid wellbore instability and fracture collapse. The hydrodynamic properties of the mud between the drill string and the wellbore are very complex due to the non-Newtonian nature of the drilling fluid, laminar or turbulent flow conditions, and eccentric rotation of the drill string. (14)

The drilling industry is continually looking for drilling fluids with improved mechanical, physical, chemical and thermal properties that are also environmentally friendly in all exploration and extraction of oil and gas fields. In order to increase drilling speed and overcome difficulties, particularly in deep **HPHT** hole drilling, including increased drag force and torque. Accurate prediction of frictional pressure losses during drilling is complicated due to the combination of different drilling parameters. (15)

II.2 Newtonian and Non-Newtonian Fluids

The relationship between shear stress (τ) and shear rate (γ) defines the flow behavior of a fluid. arrive for some liquids, this relationship is linear. If the shear rate doubles, the shear stress also doubles double. This liquid is called Newtonian liquid. An example of a Newtonian liquid is water, Alcohol and light oil. Few drilling fluids fall into the Newtonian category. Fluids with flow properties in which shear stress does not increase proportionally Liquids up to the shear rate are called non-Newtonian liquids. Most drilling fluids are of this type. (16)

II.2.1 Non-Newtonian fluids

II.2.1.1 Definition of Rheological Parameters

The rheological parameters of viscosity, shear stress and shear rate are defined in the following paragraphs.

- **Fluid Viscosity (μ)**

The viscosity (μ) of a liquid is defined as the resistance of a liquid to flow.

It can also be expressed as the resistance of a fluid to deformation when subjected to shear stress. It is mathematically quantified as the ratio of shear stress (τ) to shear rate (y). (16)

$$\mu = \frac{\tau}{\gamma} \dots\dots\dots (\mathbf{II.1})$$

The unit of viscosity is Newton seconds /m^2 or mPa. s or Centipoise.

- **Shear Stress (τ)**

This is the force that tends to cause deformation of the material by mechanical sliding along a plane parallel to the surface of the material. It can also be defined as the force required to hold a specific type of fluid through a material with a specific cross-sectional area. It is an external force acting on a material or surface parallel to the inclined plane or plane on which it lies. In laminar flow, shear stress is the frictional resistance between layers. (16)

Mathematically,

$$\textbf{Shear stress } (\tau) = \frac{\textbf{force}}{\textbf{area}} \dots\dots\dots (\textbf{II. 2})$$

It is expressed in N/m^2, (Ibl100 ft^2), Pascal or Dyncs $/cm^2$.

- **Shear Strain**

It is a dimensionless quantity used to characterize the deformation of a material due to stress. (16)

- **Shear Rate (γ)**

This is defined as the rate of change in velocity as one layer of liquid flows over an adjacent layer, divided by the distance between them.

The unit is sec-1(reciprocal seconds). If the shear rate is expressed in revolutions per minute (RPM), it can be expressed using an equation:

$$\gamma = 1.703 * RPM \dots\dots\dots (\textbf{II. 3})$$

The relationship between the shear rate and shear stress of a fluid determines how the fluid will flows (16) .

Plastic Viscosity (µp)

Plastic viscosity is a measure of the resistance of a liquid to flow, mainly caused by mechanical friction between suspended solid particles, the solid particles themselves, and the liquid phase.

It is the viscosity of a liquid at very high shear rates. In drilling, plastic viscosity is sensitive to solids concentration, thus indicating the need for dilution. This is about the ability of the drilling fluid to bring cuttings to the surface, especially in larger borehole sizes where the pump produces relatively small annular velocities.

The viscosity must be high enough to allow the sand and cuttings to settle and allow the gas to escape to the surface. Moderate plastic viscosity is required for more bit energy, higher penetration, greater annular flow for hole cleaning, low wear and low equipment fuel consumption in the circulation system. (16)

Too low plastic viscosity, however, can cause cuttings to break out of the mud and deposit behind the drill bit, causing drilling to fail. Very high plastic viscosities can be reduced by adding water (dilution) or by mechanically separating excess solids, as excessive viscosity increases pump pressure, increases slug or slug effect during tripping and restricts flow characteristics, which in turn Coming over will reduce the penetration rate. (17)

Similarly, low viscosity slurries can be reduced by adding viscosity agents such as, for example, water. g. Organoclay for oil-based mud and bentonite for water-based mud. The plastic viscosity of a liquid is defined as the difference between the viscometer readings at 600 rpm and 300 rpm, usually expressed in centipoise (cp) or millipascal seconds ($mPa.s$). (17)

Mathematically,

$$(\boldsymbol{\mu p}) = \boldsymbol{\theta_{600} - \theta_{300}} \dots\dots\dots (\mathbf{II.4})$$

The plastic viscosity of drilling fluid mainly depends on the following factors:

• Solids concentration.

•The size and shape of the solid particles present in the sludge.

•The viscosity of the liquid phase.

•Some long chain polymers are present.

•The ratio of oil to water or synthetic water in the inverse emulsion.

• The type of emulsifier in the inverse emulsion. (17)

- **Apparent Viscosity(μ_a)**

This is the viscosity of the drilling fluid at a given shear rate and fixed temperature. It is a function of the plastic viscosity and yield point of the liquid, expressed in centipoise (cp).

Understanding the apparent viscosity at high shear rates prevalent in drill nozzles is necessary to maximize permeability. Apparent viscosity is also called effective viscosity. (16)

Apparent viscosity is given mathematically by the equation:

$$\mu_a = \frac{\theta_{600}}{2} \dots\dots\dots (\mathbf{II.5})$$

- **Yield Point (Yp)**

Yield point is representative of the low shear rates present in the annulus and greatly affects the cuttings carrying capacity and annular frictional pressure drop. It is a measure of the electrochemical or attractive forces between particles in a fluid under flow conditions. It is the resistance to initial flow or the stress required in order to move a fluid. These forces are results of negative and positive charges located on or near the particle surfaces.

The yield point is sensitive to the electrochemical environment, thus indicating the need for chemical treatment of the slurry. The yield point decreases as the chemical treatment reduces the attractiveness. Lowering the yield point also lowers the apparent viscosity. It is expressed in pounds per 100 square feet($lbl100\text{ft}^2$). Mathematically, it is defined as the difference between the reading at 300 rpm and the viscosity of the plastic. (16)

The yield strength can be expressed mathematically as:

$$\tau_0 = \theta_{300} - \mu_p \dots\dots\dots (\mathbf{II.6})$$

The unit of yield point is $\text{lb}/100\text{ft}^2$.

The yield point is often affected by changes in the surface properties of liquid solids, the volume concentration of the solids, and the electrical environment (concentration and type of ions in the liquid phase) of these solids.

Yield strengths in the range of 3 to 30 $\text{lbm}/100\text{ft}^2$are considered acceptable for unweighted clay/water-based mud to improve the mud's ability to bring cuttings to the surface without increasing the mud annulus. The frictional pressure drop is sufficient to cause the formation to fracture.

The ratio (YP/PV) can be used as a measure of shear thinning behaviour of drilling fluids and the higher the ratio, the more shear thinning the fluid.

- **Gel Strength**

Gel strength describes of the mud behaviour when mud pumping is stopped. Gel strength is one of the most important drilling fluid properties because it demonstrates the ability of the drilling fluid to suspend drilling solids and weighting materials at the end of the cycle and prevent the solids from settling during tripping.

It is an important factor affecting the pressure required to cut off the cycle after the round trip and the amount of swab and surge pressure.

It is defined as the shear stress of drilling mud measured at low shear rates after the mud has been stationary for a period of time **(See figure below).** (18)

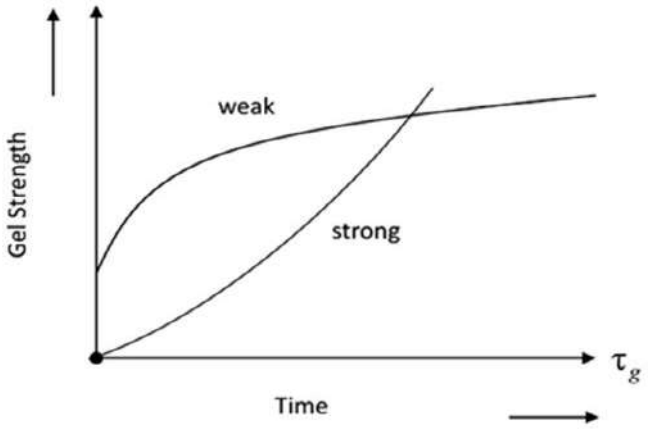

Figure II. 1- Gel strength behaviour. (19)

It is the shear stress necessary to produce a finite shear rate. While both yield point and plastic viscosity are related to the properties of moving mud, gel strength measures the properties of the mud when it is no longer moving.

Drilling fluids are thixotropic. This means that when they are not moving, they tend to form a gel structure. When the pump starts, the gel breaks and the mud becomes liquid again **(See figure just below)**.

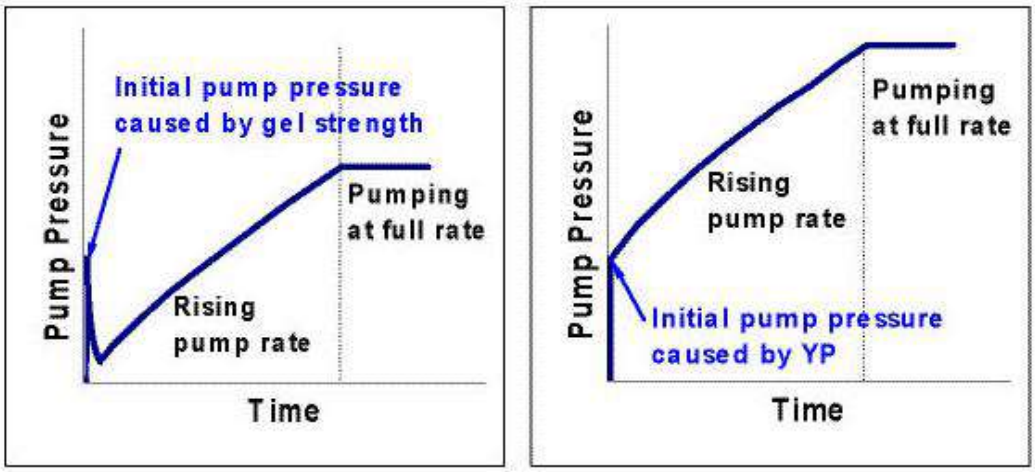

Figure II. 2- Pump pressure development caused by gel strength and yield point. (18)

These measurements are typically made and reported as initial gel strength (rest time zero) and final gel strength (rest time 10).

Two forms of gel strength are of interest, 10 second- and 10-minute gel strength. The 10-second gel strength is the maximum scale deflection observed when the cup is rotated by hand immediately after flow has stopped.

The maximum scale deviation obtained by turning on the viscometer after 10 minutes of rest is called the 10-minute gel strength.

Excessive gel requires greater pump pressure to move the fluid, and this particular situation can lead to formation damage.

The unit is $\mathrm{lb}/100\mathrm{ft}^2$.

Gel strength or yield point can be addressed by adding chemical thinners (deflocculants) such as phosphates, tannins, lignin and lignosulfonates to the drilling mud. (18)

- **Flow Behaviour Index (n)**

This is an indicator of the tendency of a fluid to shear thin and it is dimensionless. When n < 1, the fluid is shear thinning and when n > 1, the fluid is shear thickening. (20)

$$n = 3.32 \log\left(\frac{\theta_{600}}{\theta_{300}}\right) \dots\dots\dots (\mathbf{II.7})$$

- **Consistency Index Factor (K)**

This is defined as the viscosity index of the fluid system. (20)

The unit is $\mathrm{lb}/100\mathrm{ft}^2$

$$k = \frac{\tau}{\gamma^n} = \frac{\theta_{600}}{1022^n} \dots\dots\dots (\mathbf{II.8})$$

II.2.1.2 Classifications of rheological fluids

Depending on how the fluid structure responds to the applied shear forces, one can observe different types of macroscopic flow behaviour in drilling fluids such as shear thinning (pseudoplastic), shear thickening (dilatant), yield stress (visco-plastic), thixotropic, rheopectic and visco-elasticity as shown in **FigureII-3-1** and **II-3-2** below.

Classical lubrication theory of Newtonian fluids was first developed by Reynolds and has since been extended to a number of non-Newtonian fluids. (21)

- **Pseudoplastic liquid**

Pseudoplastic liquids are shear-thinning liquids that typically exhibit lower viscosity at higher shear rates. For pseudoplastic fluids (**Figure II-3-1**), the flow behavior index is typically less than 1 and n < 1.

Similarly, they show a linear relationship between shear stress and shear rate when plotted on log paper. Such as latex paint. (16)

- **Dilatant**

Dilatant fluids are shear thickening, and less common than shear thinning fluids in nature. Dilatant fluids increase their viscosity exponentially when the shear force is increased, i.e., the flow behaviour index is greater than one, $n>1$(**FigureII-2-1**).

This non-Newtonian flow behaviour has been attributed to mechanisms in which the shear stress, transmitted through the continuous medium, orients or distorts the suspended particles in opposition to the randomizing effects of Brownian motion. The apparent viscosity of dilatant fluid increases as the shear rate increases. An example of dilatant fluid is the quicksand. (16)

- **Visco-plastic or Yield Stress Fluid**

A viscoplastic fluid is one that requires a finite shear stress below which it will not flow. In other words, the fluid behaves like a rigid body at low stress, but flows like a viscous fluid at high stress.

A common example is toothpaste, where the contents will not flow out until a proper load is applied to the tube container. (16)

- **Thixotropy**

Thixotropy (**FigureII-3-2**) is a time-dependent shear-thinning property of fluids, or simply thixotropy is expressed as time-dependent pseudoplastic fluid behavior.

They are reversible and time-dependent structural changes in liquid flow behavior due to stress or loading. It arises because the microstructure of the fluid gradually collapses under shear and is reconstructed by Brownian motion. (16)

Thixotropic liquids require a finite time to reach equilibrium viscosity when subjected to sharp shear rate changes. It is generally understood as the time-dependent reduction in fluid viscosity due to limited, measurable, and reversible changes in the fluid microstructure during shear. In other words, some liquids or gels that are viscous or viscous under static conditions flow. Over time, they become thinner and less sticky when moved, compressed, shaken or sheared. Such liquids are called thixotropic liquids.

Examples include: drilling mud, clays, bentonite suspension. (16)

- **Rheopectic Fluid**

Rheopecty or rheopexy is the increase in viscosity of a non-Newtonian fluid over time when the fluid is subjected to increased shear (stress) over time. In other words, it is a time-dependent expanding liquid behavior. Examples of rheological fluids are: printing inks, gypsum pastes and lubricants. (**FigureII-3-2**). (16)

- **Viscoelastic Liquids**

Viscoelasticity is the property of a material to exhibit stickiness and elasticity when deformed. They resist shear flow and stretch linearly with time when loaded. Viscoelastic phenomena can occur in a linear regime, where the microstructure of the fluid responds linearly to stress and strain and does not change by itself, or in a

nonlinear fashion, where the microstructure changes in response to applied stress and strain. but reversible. (16)

A good example of a viscoelastic fluid is a polymer fluid.

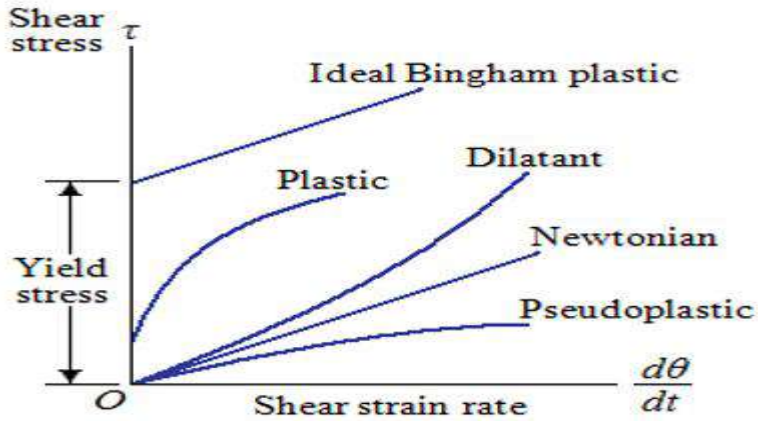

Figure II.3. 1- Shear Stress Versus Shear rate for Newtonian and new Newtonian fluids. (16)

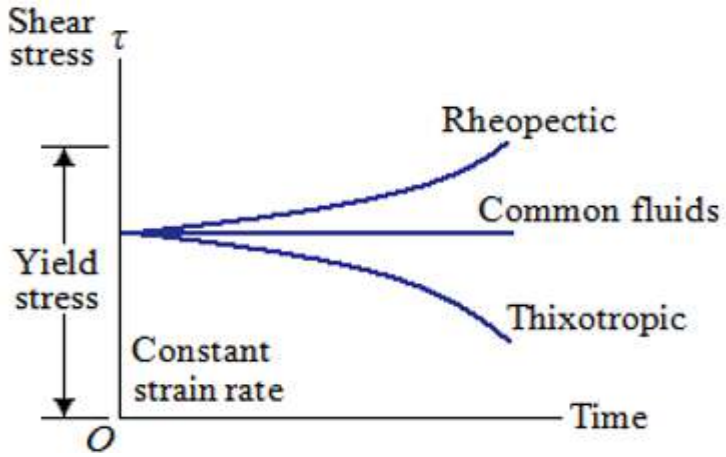

Figure II.3. 2- Shear Stress Versus Shear rate for thixotropic and rheopectic fluids. (16)

II.3 Rheology

One of the most influential properties of a drilling fluid is its viscosity. Understanding the role of viscosity in drilling and other operations and the ability to match viscosity requirements to prevailing conditions for that requirement is a key factor in optimizing fluid efficiency. In the early 20th century, the properties of many non-Newtonian fluids prompted Professor Eugene Bingham to develop the term rheology, which he defined as the study of the deformation and flow of matter.

The term rheology is derived from the Greek rheo, meaning flow, and logus, meaning science or research. Deformation is the relative displacement of points on an object.

It is divided into two types **(See figure below):**

- elasticity and flow.
- Elasticity is reversible deformation.

the deformed body returns to its original shape and the work done is largely recoverable. Flow is irreversible deformation; the material does not return to its original shape when the stress is removed. This means that work is converted to heat. Viscoelastic materials exhibit both elasticity and fluidity. (22)

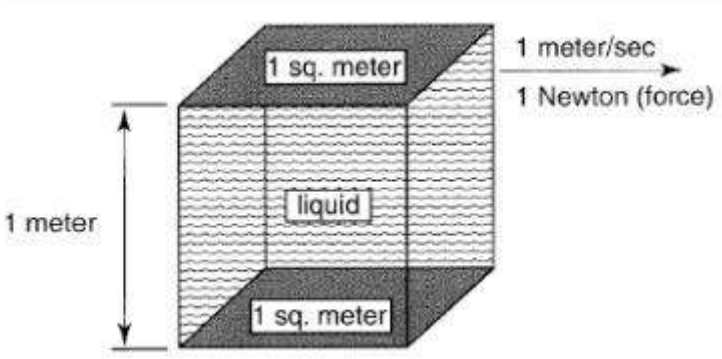

Figure II. 3- Diagram for Rheological Definitions. (22)

The units of shear stress are Newtons per square meter, also known as Pascals. Alternative units for shear stress are dynes per square centimeter and pounds force per square inch. Shear Rate($\dot{\gamma}$) is defined as the rate of movement of the fluid between the plates. It is determined by dividing the velocity difference between the plates by the distance between them.

This can also be called the velocity gradient. In this case, the shear rate or velocity gradient is one meter per second per meter of fluid and is thus measured in reciprocal seconds($\sec^{-1}$).

Viscosity (μ) is defined as the ratio of shear stress over shear rate. Consequently, the units are Newton seconds per square meter or Pascal seconds.

Another common unit is the Poise (dyne second/centimeter^2). One centipoise is equal to one milli Pascal second ($1cP = 1\ mPa.s$).

When you learn about drilling mud, the rheological models are essential knowledge. The rheological models are critical for a drilling fluid study because they are used to simulate the characteristics of drilling mud under dynamic conditions. With this knowledge, you will be able to determine some of the key figures, such as equivalent circulating density, pressure drops in the system, and hole cleaning efficiency.

The drilling fluid has three flow regimes, plug flow, laminar flow and turbulent flow and **(Figure II.4)** demonstrates 3 flow regimes on the shear rate and shear stress curve. In between each zone, there is a transition zone where the flow regimes are changing. (22)

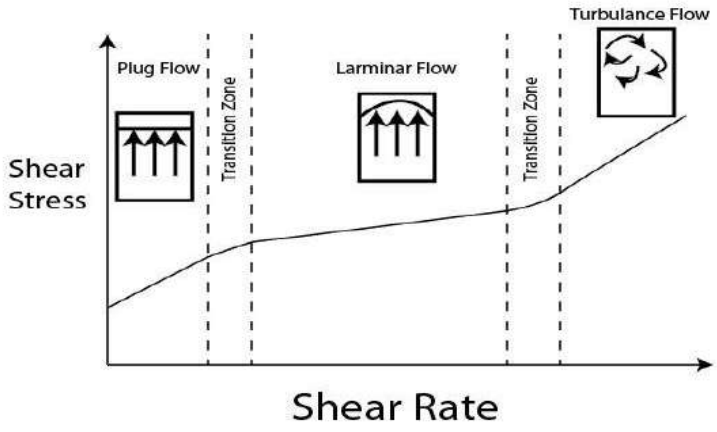

Figure II. 4-the shear rate and shear stress curve on flow regimes, plug flow, laminar flow, and turbulent flow. (19)

II.3.1 Flow regimes

II.3.1.1 Plug Flow

Plug flow happens only with a very low shear rate and when the mud is in a gel stage. The velocity of the mud at the center of the annulus is equal to the velocity at the sides. (19)

II.3.1.2 Laminar Flow

The laminar flow usually occurs at a low flow velocity and it is best understood by considering mud as being layers of fluid flow. The velocity of the mud in the center is moving the fastest and the velocity of an adjacent layer moves slower.

At the edge of the pipe, the velocity is very low when compared to the velocity in the center. For the laminar flow, the flow has a predictable pattern, and the shear rate is a function of the shear stress of the fluid.

Therefore, the equations used for the laminar flow are based on fluid flow models, such as Newtonian, Bingham Plastic, and Power Law. (19)

II.3.1.3 Turbulence Flow

Fluid moving in a turbulence flow region is subject to random local fluctuations in both the direction of flow and fluid velocity. For the turbulent flow, it is difficult to find the proper equations to describe the fluid flow models because the flow at this stage is disorderly. Practically, most people use empirical equations to figure out the flow relationship for this flow regime. (19)

Things to remember include that the drilling mud does not follow each particular fluid model exactly; however, either one or more fluid models can be utilized to predict the flow behavior of drilling mud and as a result it is still within a reasonable range. (19)

II.3.2 Rheological classification

Table II. 1- shows a simplified rheological classification based on the criteria discussed in section. (23)

Fluid / Flow	Viscous		Viscoelastic
Transient	Response time = 0		Response time ≠ 0
Laminar	Newtonian	Non-Newtonian	Non-Newtonian
Turbulent			Decrease in pressure losses
Rest	Non thixotropic	Thixotropic or non-thixotropic	

II.3.3 Rheological Parameters Measurement

There are two types of viscometers that are used for rheological parameter measurement. These are: Marsh Funnel Viscometer and Direct Indicating Viscometer.

II.3.3.1 Marsh Funnel Viscometer

The Marsh Funnel viscometer is an instrument for measuring the viscosity of mud sample on the rig during drilling operation on a regular basis. The apparatus set up for viscosity measurement consist of a Marsh funnel, a measuring cup graduated in cubic centimeters for receiving the fluid as it flows out of the funnel, a stop watch for measuring the elapsed time for fluid movement and a thermometer for measuring the temperature of the sample.

The procedure is to fill the funnel with the mud sample up to the screen level and to then observe the number of seconds required for one quart (946ml) of the mud sample to flow out of a full Marsh funnel **(See figure II. 5).**

Funnel viscosity is the ratio of the speed of the sample fluid as it passes through the outlet tube (the shear rate) to the amount of force (the weight of the fluid) that is causing the fluid to flow (the shear stress). (24)

Figure II. 6- Fann Marsh Funnel Viscometer model 201

II.3.3.2 OFITE-8-Speed Rotational Viscometer

The OFITE model 800,8-speed viscometer is used for the determination of the rheological characteristics of drilling muds and cement at atmospheric pressure (14.7 $psia$). It has a simple speed control knob and a lighted dial for easy dial reading.

- **Experimental Procedure for Determining Mud Samples Viscosity from 8-Speed Viscometer(See figure below):**

1. Agitate the mud sample for a sufficient period of time by using the multi-mixer to prevent sagging of mud components.
2. Calibrate the viscometer with specified fluid by the manufacturer.
3. Pour the agitated mud sample into the mud cup and place it on the viscometer platform under the sleeve and ensure that the pins at the bottom of the cup fit into the holes in the base plate.
4. Turn the knurled knob between the rear support to raise or lower the platform until the rotor sleeve is immersed in the mud sample up to the scribed line.
5. Re-stir the mud sample for few minutes and turn the control knob to the desired rotor speed.
6. Allow the dial reading to stabilize and record the corresponding dial reading at the set rotor speed.
7. Repeat the aforementioned steps for other rotor speeds. (24)

Figure II. 7- OFITE 8-Speed Rotational Viscometer. (24)

II.3.4 Rheological models drilling fluids

Rheological models are mathematical equations that describe the flow behaviour of the fluids in the drill pipe and annulus during oil and gas drilling operations. These models are used to characterize flow properties with a view to determining the ability of a fluid to perform specific functions and they are of utmost importance in correct estimation of pump pressure and equivalent circulating density under downhole conditions.

Drilling fluid rheological model can be broadly divided into the Newtonian model and the non-Newtonian model.

Several mathematical models have been developed to describe the shear stress/shear rate relationship on non-Newtonian fluids. These models are used to characterize flow properties in an effort to determine the ability of a fluid to perform specific functions.

Misapplication of rheological data can result in an over-simplification or exaggeration of fluid features, accompanied by the failure to perform a specific task. In order to optimize fluid performance, an in-depth discussion of data acquisition, rheological models and their inherent limitations is necessary. (25)

The rheological model for non-Newtonian fluids may be grouped under three categories. These are, the empirical model which are derived from examination of experimental data and an example is Power law rheological model**,** the structurer model such as the Hershel-Bulkley model. (26)

Also, there is theoretical model which indicates factors that influences a rheological parameter and examples are, the Krieger-Dougherty model for relative viscosity, and the Bingham Plastic model**.** (27)

Other mathematical models used in describing the rheology of non-Newtonian fluids are premised on the modification of anomalies associated with the basic models.

Selection of the best rheological model that accurately represent the shear stress-shear rate analysis is achieving correct results for pressure drops and hydraulic calculations.

Measurement of rheological properties also makes possible mathematical descriptions of circulating fluid flow that are important for the following hydraulics-related determinations. (28)

1. Calculating frictional pressure losses in pipes and annuli.
2. Determining equivalent circulating density (ECD) of the drilling fluid under downhole conditions.
3. Determining flow regimes.
4. Estimating hole-cleaning efficiency.
5. Estimating swab/surge pressures.
6. Optimizing the drilling fluid circulating system to improve drilling efficiency.

II.3.4.1 Newtonian fluids

The shear stress of Newtonian fluids is directly proportional to the shear rate: if one variable is doubled, the other one is doubled also. The rheological equation is

$$\tau = \mu\gamma \ldots\ldots\ldots (\mathbf{II.9})$$

The following plot is obtained in Cartesian coordinates (**FigureII-7**).

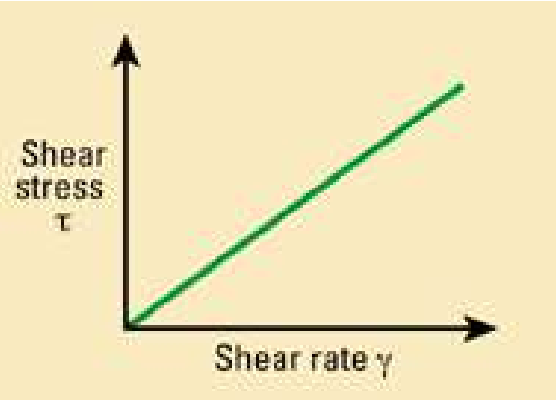

Figure II. 8-Newtonian fluids behaviour.

The graph is a straight line passing through the origin; the fluid begins to move as soon as a nonzero force is applied. Examples of such fluids are water or gasoline.

For a Newtonian fluid, the ratio $\mu_a = \frac{\tau}{\dot{\gamma}}$ is constant at constant temperature and pressure, and is the viscosity. (22)

II.3.4.2 Non-Newtonian fluids

We shall discuss only three types of non-Newtonian fluids which are most often encountered in drilling muds and cement slurries. (22)

- **Bingham Model**

In Bingham plastic fluids the shear stress also varies linearly with shear rate but, unlike Newtonian fluids, a minimum force must be applied to impart motion to them. This force, is known as the yield-point or yield-value. Such fluids are characterized by two constants:

- Yieldpoint or yield-value τ_0 which corresponds to the smallest force required to set the fluid in motion.
- Plastic viscosity, μ_p which is the ratio between the increment in the shear stress and the corresponding increment in the shear rate.

the slope of the curve obtained by plotting τ as a function of $\dot{\gamma}$.

The theoretical equation of flow of such fluids is:

$$\boldsymbol{\tau = \tau_0 + \mu_p \dot{\gamma}} \ldots\ldots\ldots (\mathbf{II.10})$$

Where:

$\tau =$ Shear stress
$\tau_0 =$ Yield point
$\mu_p =$ Plastic viscosity
$\dot{\gamma} =$ Shear rate

The presence of a yield stress means that a certain critical shear stress must be exceeded before flow can begin. If the fluid exhibits a linear increase in shear stress

with shear rate after the yield value is exceeded, it is called a Bingham Plastic fluid. While some fluids exhibit a yield point, most oil field fluids show shear rate dependence after flow is initiated.

This model is interesting but not very useful in describing the behavior of polymer or invert emulsion fluids. In the oil field, the Bingham Plastic model has been used to describe the behavior of some clay-based drilling fluids and a few cement slurries. An extension of the Bingham Plastic model to include shear rate dependence is the Herschel-Bulkley model, described later. (22)

There are several models that involve the use of three or more adjustable parameters. It is necessary to include a third parameter to describe the flow of fluids in the upper or lower Newtonian region as well as the power law region. (22)

- ✓ **Determination of plastic viscosity μ_p and yield-point τ_0**

These determinations are carried out in a Fann viscometer according to ***API RP 13B***. The values to be determined are the shear stress $\dot{\gamma}_2 = 1020\ s^{-1}(at\ 600\ rpm)$, and the shear stress τ_{510} at the shear rate $\dot{\gamma}_1 = 510\ s^{-1}$(at 300 rpm).

- ✓ **Determination of the plastic viscosity μ_p (See figure II.8-10)**

In SI units, we have:

$$\mu_p = \frac{\tau_{1020} - \tau_{510}}{1020 - 510} \dots\dots\dots (II.11)$$

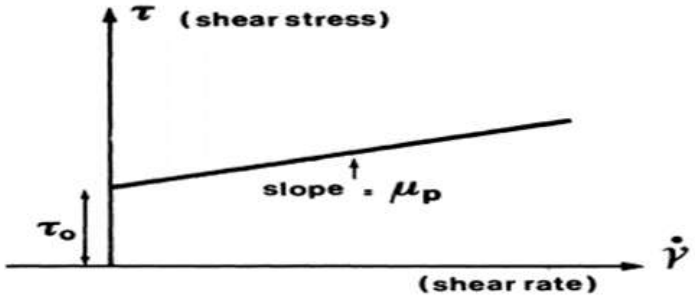

Figure II. 9- Bingham fluid theoretical flow curve. (22)

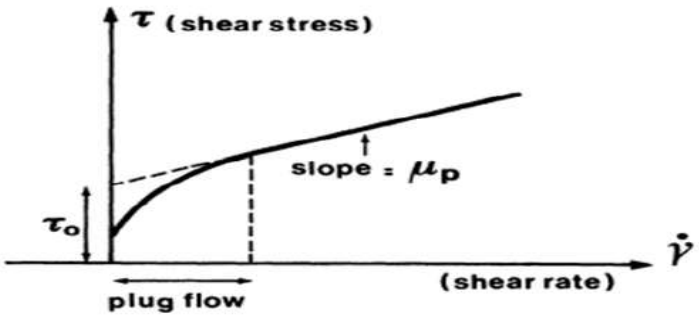

Figure II. 10- Bingham fluid experimental flow curve. (22)

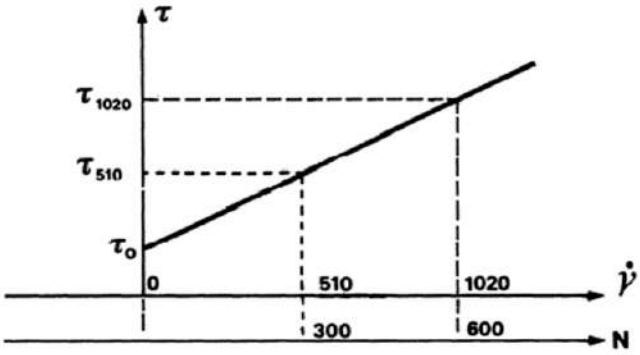

Figure II. 11-Determination of Bingham fluid rheological parameters.

If μ_p is expressed in centipoises, we have:

$$\mu_p = \frac{0.51(\theta_{600} - \theta_{300})}{1020 - 510} 1000 = \theta_{600} - \theta_{300} \quad \ldots\ldots\ldots (II.12)$$

i.e., μ_p (cP} = Fann reading at 600 rpm - Fann reading at 300 rpm.

- ✓ **Determination of the yield-point τ_0**

It is apparent from the (**figure II-11)** that

$$\tau_0 = \tau_{1020} - 2(\tau_{1020} - \tau_{510}) \quad \ldots\ldots\ldots (II.13)$$

or, if $\tau_0$is expressed in$1b/100ft^2$ and μ_a and μ_p in cP,

$$\tau_0 = \theta_{600} - 2(\theta_{600} - \theta_{300})$$
$$= \theta_{600} - 2\mu_p$$
$$= 2(\mu_a - \mu_p)$$

- **Power Law Model (Pseudo-plastic or power-law fluids)**

One of the more widely used models for describing the behavior of oil field fluids is the power law model. This model (Equation 2.14) is valid for the linear, i.e., center section, of the curve shown in (**Figure II.11-12).**

In the power law model, the viscosity term from the Newtonian model is replaced with a constant, K, termed the consistency index, which serves as a viscosity index of the system. The consistency index has the unusual set of units, Force-sec / Area.

In addition, the shear rate term is raised to the n^{th} power, thus the term power law. The factor, n, is called the power law index which indicates the tendency of the fluid to shear thin. As the value of the flow behavior index deviates from one, the fluid becomes increasingly non-Newtonian. (22)

Where:

$$\boldsymbol{\tau = K\dot{\gamma}^n} \text{ ... ... } \textbf{(II. 14)}$$

$\tau =$ Shear stress
$K =$ Consistency index
$\dot{\gamma} =$ Shear rate
$n =$ Power law exponent

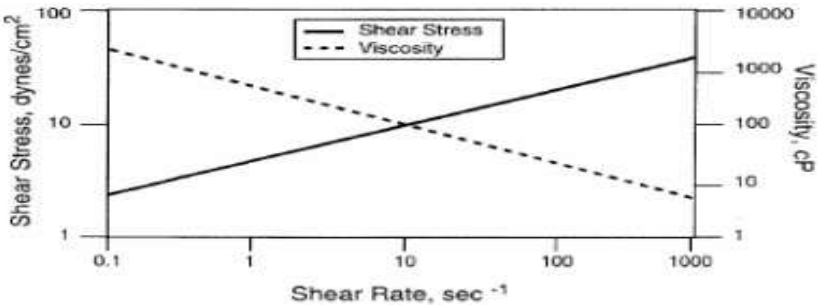

Figure II. 12-Idealized Power Law Fluid. (22)

When the log of the shear stress is plotted against the log of the shear rate (Figure 12), a straight line with a slope equal to n and an intercept (at a shear rate of one) equal to log K, results. A plot of the log of the viscosity versus log of the shear rate also results in a straight line.

Most polymer solutions and invert emulsion drilling fluids are pseudoplastic. In this case, increased shear rate causes a progressive decrease in viscosity. This is due to alignment of the polymer chains, or structural elements of the fluid, along the flow lines. For pseudoplastic fluids, the value of the flow behavior index, n, ranges from about 0.1 to < 1.0. When the n value is equal to 1.0, the power law reduces to the Newtonian model.

The further that n is reduced from 1.0 the more the fluid deviates from Newtonian behavior. Although this is one of the most popular models used, no known fluid exhibits power law behavior over the entire range of shear rate conditions. Therefore, the primary drawback is the limited shear rate range over which it is valid. Care must be taken to use data within the power law region to accurately calculate parameters (n and K). For example, with xanthan gum, calculating n and K from $600\ rpm$ ($1022\ sec-1$) and $300\ rpm$ ($511\ sec-1$) on a concentric cylinder viscometer, will result in inaccurately high n and low K values as compared to values obtained at lower shear rate.

Pseudo-plastic fluids, like Newtonian fluids, will flow under any applied stress, however small. But, as distinct from Newtonian fluids, the shear stress is not proportional to the shear rate, but to its n^{th} power; hence the name power-law fluids. The equation of flow is:

$$\boldsymbol{\tau = K\dot{\gamma}^{n}} \ldots\ldots\ldots (\mathbf{II.15})$$

where $\boldsymbol{K}$ is the consistency index in $\mathrm{Pa.S}^{n}$ or in $\mathrm{lb.s}^{n}/100\mathrm{ft}^{2}$, and n is the dimensionless flow behavior index, which is unity or smaller than unity.

If $n = 1$, the equation becomes identical with the equation offlow of a Newtonian fluid having the viscosity K.

The following graphs shown in Figure 14 are flow curves of power-law fluid in Cartesian and logarithmic coordinates respectively. (22)

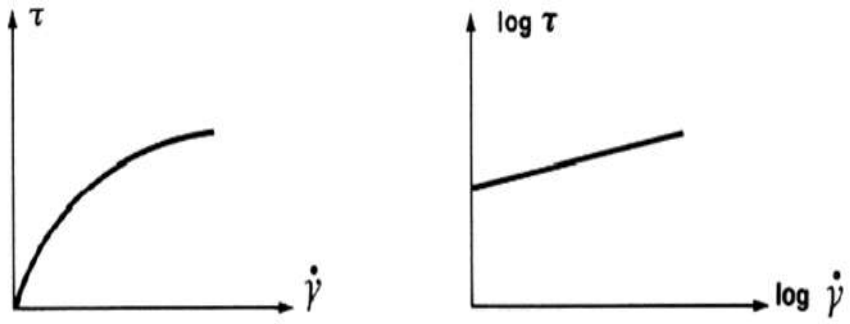

Figure II. 13-Power-law fluid flow curve. (22)

- ✓ **Determination of flow behavior index n and consistency index K in a Fann viscometer:**

Power Law Constants, n and K as described above, the consistency factor, K, describes the thickness of the fluid and is somewhat analogous to the effective viscosity.

The flow behavior index, n, indicates the degree of non-Newtonian behavior. These two constants can be calculated from any two values of shear rate/shear stress relationships. When readings are obtained from a V-G meter at 600 rpm, 300 rpm, and 3 rpm, two sets of n and K can be developed corresponding with fluid flow inside the drill pipe and fluid flow in the annulus.

This is done to improve the accuracy of hydraulic calculations in the drill pipe or annulus since the Power Law Model does not exactly describe the behavior of drilling fluids. To obtain the power law constants corresponding to fluid flow inside the drill pipe, the 600 rpm and 300 rpm readings are used.

The determinations made in a six-speed Fann viscometer (or, if this instrument is not available, in a two-speed Fann viscometer, using also g_0 , which is considered to represent a determination at 3 rpm) are plotted, as a rheogram, on log-log paper, shear

rates (in s^{-1}) being plotted on the abscissa, shear stresses (in $lb/100ft^2$) on the ordinate (Figure II. 13). (22)

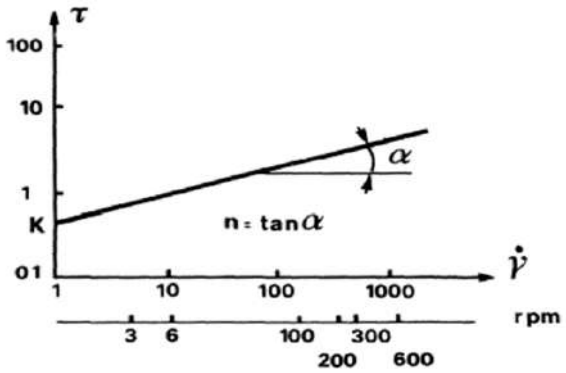

Figure II. 14-Determination of power-law fluid rheological parameters. (22)

✓ **Determination of n**

We have seen that:

$$n = \frac{\log \tau/\tau'}{\log \dot{\gamma}/\dot{\gamma}'} \text{ ..... (II.16)}$$

If $\dot{\gamma} = 2\dot{\gamma}'$, we have:

$$n_p = \frac{\log \tau/\tau'}{\log 2} = \frac{\log \theta/\theta'}{\log 2} = 3.32 \log \frac{\theta}{\theta'} \text{ ... ... (II. 17)}$$

$$n_p = 3.32 \log \left(\frac{\theta_{600}}{\theta_{300}}\right)$$

$$= \frac{5.11 \times \theta_{600}}{1022^{n_p}}$$

$\dot{\gamma}_2 = 1020\text{s}^{-1}$(at 600rpm)
$\dot{\gamma}_1 = 510\text{s}^{-1}$(at 300rpm)
$n = 3.32\log \frac{\text{Fann reading at 600rpm}}{\text{Fann reading at 300rpm}}$

To obtain he power law constants corresponding to fluid flow in the annulus, the 300 rpm and 3 rpm (or initial gel strength) readings are used. (22)

$$n_a = 0.5\log\left(\frac{\theta_{300}}{\theta_3}\right)$$
$$K_a = \frac{5.11 \times \theta_{300}}{5.11^{n_a}}$$

Where,

$K =$ consistency factor, poise.

$n =$ flow behavior index, dimensionless.

- ✓ **Determination of K**

$$\boldsymbol{K = \frac{\tau}{\dot{\gamma}^n}} \ldots\ldots\ldots (\textbf{II. 18})$$

If $\dot{\gamma} = 1, K = \tau_1$

If τ is given in $\text{lb}/100\text{ft}^2$ and$\dot{\gamma}$ in s^{-1} ,

the unit of K will be $\text{lb.s}^n/100\text{ft}^2$

Ifτ tis given in pascal the unit of K will be $\text{Pa} \cdot \text{s}^n$ It will be recalled that

$1\text{lb}_{\text{force}}/100\text{ft}^2 = 0.478964\text{Pa}$.

- **Herschel-Bulkley Model**

Fluids that exhibit a yield point and viscosity that is stress or strain dependent cannot be adequately described by the Bingham Plastic model. The Herschel-Bulkley

model **(Figure II. 14)** corrects this deficiency by replacing the plastic viscosity term in the Bingham Plastic model with a power law expression (Equation 4). (22)

$$\boldsymbol{\tau = \tau_0 + K\dot{\gamma}^n} \ldots\ldots\ldots (\mathbf{II.19})$$

Where:

$\tau =$ Shear stress
$\tau_0 =$ Yield point
K = Consistency index
$\dot{\gamma}^n =$ Power law expression

This model is useful for describing a wide range of fluids used in oil field operations. The model is reduced to the power law if there is no yield stress and to the Bingham model if n = 1. The primary limitation of this and all other models that cannot be linearized is curve fitting to evaluate model parameters.

Computers and non-linear curve fitting techniques have overcome this problem. Many publications have shown the usefulness of the three parameter Herschel-Bulkley model and this model is generally accepted as the best available for describing the flow properties of drilling fluids. (22)

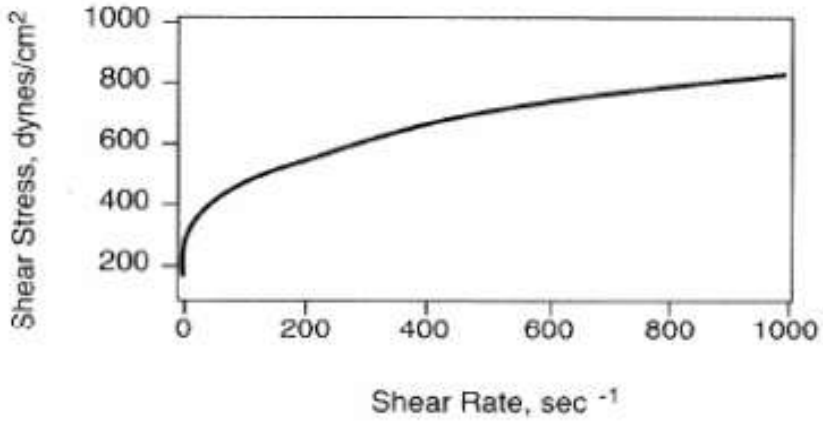

Figure II. 15- Idealized Herschel-Bulkley Flow. (22)

II.3.5 Rheological Models in advantage

In Advantage Reporting it is possible, and recommended, to input at least Fann readings for 600, 300, 200, 100, 6 and 3 rpm. The 10 second, 10 minute and 30-minute gel strengths are also entered. From these numbers the Plastic Viscosity and Yield Point are derived along with n and k for the power law model.

The hydraulics equations in Advantagesm Reporting are **API 13-D** equations and utilize the power law. These equations do not account for the effect of temperature and pressure on fluid density and rheological properties.

This means that in most situations that the results will contain inaccuracies. It is important to be aware of this and the causes of the inaccuracies.

In Advantagesm Engineering there are two hydraulics models – the BP model and the BHI model. These two models and the rheological models they use will now be discussed separately. (22)

II.3.5.1 BP Model

The desired input parameters are the Fann readings – preferably at least the 600, 300, 200, 100, 6 and 3 rpm readings - plus the 10 second- and 10-minute gels. If only Plastic Viscosity and Yield Point are entered instead of the Fann readings the Bingham model will be used for hydraulics equations. If the Fann readings are entered, then Herschel Bulkley will be used for pressure loss calculations. The cuttings concentration in the drilling fluid is not taken into account in ECD calculations.

The BP model does not allow for temperature and pressure effects on fluid density and rheological properties. (22)

II.3.5.2 BHI Model

The Herschel Bulkley model most accurately model drilling fluids,being the recommended model for calculating pressure losses. It is not advisable, nor technically correct, to change models in order to get the best fit between modeling results and field data. In the BHI model it is possible to use Fann 35 data or Fann 75 data, though the

latter is more accurate, especially when using invert emulsion drilling fluids. In Spreadsheet Hydraulics the Fann 35 readings are used and system and bit pressure losses are calculated at ten different flow rates using the selected model. The Calc. Fann Fit button can be selected in order to check which model best fits the viscometer readings.

The default model in the hole cleaning mode for annular pressure loss calculations is the Herschel Bulkley model. A selected model can be used to calculate drill string and drill bit pressure losses. In System Mud Hydraulics with Hole Cleaning Herschel Bulkley is used for annular pressure loss calculations using the input flow rate.

In the HT-HP mode Fann 70 / 75 data must be entered corresponding to the temperature and pressure conditions in the well. When hole cleaning is taken into account the Herschel Bulkley model is used to calculate annular pressure losses, but the manually selected model is used for all other pressure losses. In this mode either spreadsheet Hydraulics or System Mud Hydraulics may be selected. (22)

II.4 Pressure loss calculations in wellbores

There are several ways to examine prediction of pressure losses in the circulating system. Note that for non-Newtonian modeling, both the friction factor estimation and the transition to turbulent flow are more difficult, leading to the use of largely empirical equations for pressure loss calculations **(See table below)**.

These predictive equations are helpful, but sometimes result in large errors, and should be calibrated with data from the actual well once drilling has commenced. Note that some portions of the circulation system can be calculated with greater accuracy than others. Bit pressure losses are generally thought to be the most accurate component, followed by surface system losses and then inside-drill string losses.

The least accurate predictions are those used in the annular pressure losses. There are two primary geometries and four fluid models to consider. The geometry is that of a pipe for flow inside the drill string traveling to the bit and an annulus (which can also be either concentric or eccentric to varying degrees).

The fluid models commonly used for prespud design include Newtonian, Bingham Plastic, and Power Law. These can be further expanded as the designer desires to look at laminar flow and turbulent flow conditions. (29)

To summarize, the different geometries, fluid models, and flow characteristics to be used, most with a separate formula for computing pressure loss. Note that in the absence of a compelling reason to use something else, the power law models will generally give more accurate results and are recommended.

However, the Newtonian and Bingham plastic equations are given for completeness. The well designer should determine the geometry he/she is dealing with, estimate whether the flow is laminar or turbulent, and then use the power law equation for that pair of criteria. Equations for these different cases will be given without much discussion below. For a full discussion of any of these equations, please refer to the chapter endnote references themselves. Due to increased importance of the bit nozzle pressure losses. (29)

Table II. 2- Flow geometries, models, and regime combinations.(30)

Geometry	Flow model	Flow regime
Pipe	Newtonian	Laminar
Pipe	Bingham plastic	Laminar
Pipe	Power flow	Laminar
Pipe	Newtonian	Turbulent
Pipe	Bingham plastic	Turbulent
Pipe	Power flow	Turbulent
Annulus	Newtonian	Laminar
Annulus	Bingham plastic	Laminar
Annulus	Power flow	Laminar
Annulus	Newtonian	Turbulent
Annulus	Bingham plastic	Turbulent

II.4.1 Drill string and annular hydraulics

This section on drill string and annular hydraulics is designed to create a basic understanding of how the various calculations are carried out. The discussion below is based on the use of the power law rheological model.

In Advantage Engineering, the rheological model can be selected and this directly affects hydraulics calculations as different values are derived for the various factors using the different models. The most commonly used models are the Herschel-Bulkley and is recommended as it is capable of fitting data from power law fluids, Bingham Plastic fluids and power law fluids with a yield stress. (30)

II.4.1.1 Fluid Velocity

The flow of drilling fluid through the surface equipment, drill string, and annulus may be considered to be flow through a series of circular pipes. The diameter and cross-sectional area in each portion of the circulating system vary from one part to the other. If the volumetric flow rate through the circulating system remains constant, then the speed or velocity of the drilling fluid changes in relation to the cross-sectional area for that particular part of the system.

The highest velocities occur where the diameter is the smallest. The fluid velocity is the first and most important step in making hydraulic calculations in the drilling operation. (30)

- **For fluid velocity in the drill string,**

$$V_p = \frac{0.408Q}{D^2} \dots\dots\dots (II.20)$$

where:

$V_P =$ fluid velocity in pipe, ft/sec

Q = volumetric flow rate, gal/min

$D =$ inside diameter of the pipe, in.

- **For fluid velocity in the annulus,**

$$V_a = \frac{0.408Q}{(D_2)^2 - (D_1)^2} \dots\dots\dots (\text{II. 21})$$

where:

$V_a =$ annular velocity, ft/sec
$Q =$ volumetric flow rate, gal/min
$D_2 =$ hole diameter, in.
$D_1 =$ outside diameter of the drill pipe/collar/etc, in.

Note that the above equations describe average flow rate in the drill string and the annulus. In the annulus on a directional well there will be a series of velocities in the annulus. (**Figure II. 16)** illustrates the fluid velocity distribution in an eccentric annulus with a rotating inner cylinder. This is the type of flow pattern to be expected in a deviated well. (31)

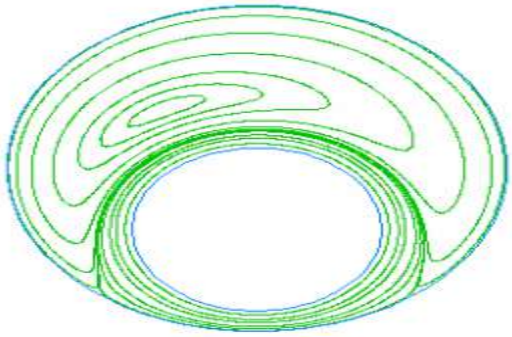

Figure II. 17- Flow in an Eccentric Annulus with inner cylinder rotation. (32)

II.4.1.2 Reynolds Number

After calculating the effective viscosity, μ_e, as a function of fluid velocity and power law constants, the Reynolds Number is calculated to determine the flow regime of the fluid (i.e., laminar, transitional, or turbulent flow). (32)

The equation for **Reynolds Number** inside the pipe is:

$$R_p = \frac{928(V_p)(D_p)\rho}{\mu_{e_p}\left[\frac{3n_p+1}{4n_p}\right]n_p} \quad \ldots\ldots\ldots (\mathbf{II.22})$$

where:

Re_p = Reynolds Number inside the pipe

V_p = fluid velocity inside the pipe, ft/sec
D_p = inside diameter of the pipe in.
ρ = fluid density, lb_m/gal
μ_{e_p} = effective viscosity inside pipe , cp
n_p = power law constant for pipe

To obtain the Reynolds Number in the annulus:

$$Re_a = \frac{928V_a(D_2 - D_1)\rho}{\mu_{e_a}\left[\frac{2n_a+1}{3n_a}\right]^{n_a}} \quad \ldots\ldots\ldots (\mathbf{II.23})$$

where:

Re_a = Reynolds Number in the annulus

V_a = fluid velocity in the annulus, ft/sec

D_2 = hole diameter, in.
D_1 = outside pipe diameter, in.
ρ = fluid density, lb_m/gal
μ_{e_a} = effective viscosity in the annulus, cp
n_a = power law constant for the annulus

II.4.1.3 Friction-Loss Pressure Gradient

The total pressure required to circulate the drilling fluid includes not only the pressure drop across the bit nozzles, but also the friction losses throughout the surface system, drillstring, and annular sections.

The appropriate friction factor (from previous section) is substituted into the Fanning equation to determine the friction-loss pressure gradient. The appropriate values must be used for each section of pipe or annulus sections with different diameters. (32)

- **Friction-Loss gradient in pipe:**

$$\frac{\mathbf{P_p}}{\mathbf{L_m}} = \frac{(\mathbf{f_p})(\mathbf{V_p})^2(\boldsymbol{\rho})}{\mathbf{25.81D}} \ldots\ldots\ldots (\mathbf{II.24})$$

Where:

$\frac{P_p}{L_m}$ = pressure loss per measured depth, psi /ft

and,

f_p = friction factor (laminar, transitional, or turbulent)

V_p = bulk velocity in pipe, ft/sec

ρ = fluid density, lb_m/gal

D = inside diameter of pipe, in.

- **Friction-loss gradient in annulus:**

$$\mathbf{P_a} = \frac{\mathbf{P_a}}{\mathbf{L_m}} \times \textbf{ Annular Length } \ldots\ldots\ldots (\mathbf{II.25})$$

$$\frac{P_a}{L_m} = \frac{(f_a)(V_a)^2(\rho)}{25.81(D_2 - D_1)}$$

Where:

$\frac{P_a}{L_m}$ = pressure loss per measured depth, psi / ft

f_a = friction factor (laminar, transitional, or turbulent)

V_a = bulk velocity in annulus, ft/sec

$\rho =$ fluid density, lb_m/gal

$D_2 =$ hole diameter, in.

$D_1 =$ outside pipe diameter, in.

II.4.1.4 Equivalent Circulating Density

The pressure required to overcome the total friction losses in the annulus, when added to the hydrostatic pressure of the fluid, gives the Equivalent Circulating Density (ECD) as follows. (22)

$$\mathbf{ECD} = \frac{\mathbf{\Sigma P_a}}{(\mathbf{.052})(\mathbf{TVD})} + \boldsymbol{\rho} \dots\dots\dots (\mathbf{II.26})$$

Where**:**

ECD = equivalent circulating density, lb_m/gal

$\Sigma P_a =$ sum of the friction loss in all annular intervals, psi

TVD = true vertical depth, ft

$\rho =$ fluid density, $lb_m/$ gal

Note: Temperature and pressure affect both the density of fluids and their rheological properties, both of which affect the ECD. (22)

II.5 Conclusion

Several mathematical models used in describing the rheology of non-Newtonian fluids include but not limited to the following: The Bingham Plastic Model, the Power Law Model, Herschel-Bulkley Model. Selection of the best rheological model that accurately represents the shear stress-shear rate analysis is sine qua non to achieving correct results for pressure drops and hydraulic calculation.

CHAPTER

III

THE FINITE VOLUME METHOD

III. Chapter III

III.1 Introduction

The Finite Volume Method (FVM) is a numerical technique that transforms the partial differential equations representing conservation laws over differential volumes into discrete algebraic equations over finite volumes (or elements, cells or meshes).

The first step in the solution process is the discretization of the geometric domain, which, in the FVM, is discretized into non-overlapping elements or finite volumes.

The system of algebraic equations is then solved to compute the values of the dependent variable for each of the elements.

Finally, in the FVM it is quite easy to implement a variety of boundary conditions in a noninvasive manner, since the unknown variables are evaluated at the centroids of the volume elements, not at their boundary faces.

These characteristics have made the Finite Volume Method quite suitable for the numerical simulation of a variety of applications involving fluid flow and heat and mass transfer, and developments in the method have been closely entwined with advances in CFD.

From a limited potential at inception confined to solving simple physics and geometry over structured grids, the FVM is now capable of dealing with all kinds of complex physics and applications. (32)

III.2 The Energy Equation

For a steady low-velocity flow with negligible viscous dissipation, the energy equation can be written as:

$$\mathbf{div}\,(\boldsymbol{\rho}\mathbf{uh}) = \mathbf{div}\,(\mathbf{k}\,\mathbf{grad}\,\mathbf{T}) + \mathbf{S}_{\boldsymbol{n}} \ldots\ldots\ldots (\mathbf{III.1})$$

Where

- h is the specific enthalpy
- k is the thermal conductivity
- T is the temperature
- Sn is the volumetric rate of heat generation.

The term $div\ (k\ grad\ T)$ represents the influence of conduction heat transfer within the fluid, according to the Fourier law of conduction. (33)

For incompressible fluids we have:

$$\mathbf{c\ grad\ T\ =\ grad\ h} \dots\dots\dots (\mathbf{III.2})$$

Where c is the constant specific heat. With this substitution, the energy equation becomes:

$$\mathbf{div\ (\rho uh) = div\left(\left(\frac{k}{c}\right) grad\ h\right) + S_h} \dots\dots\dots (\mathbf{III.3})$$

If c is constant, the $h \sim T \Rightarrow h = ct$,

Wich lead to:

$$\mathbf{div\ (\rho uT) = div\left(\left(\frac{k}{c}\right) grad\ h\right) + \frac{S_h}{c}} \dots\dots\dots (\mathbf{III.4}$$

The constant heat-conduction term is obtained when we set the velocity u to zero, so,

$$\mathbf{div\ (k\ grad\ T) + Sn\ =\ 0} \dots\dots\dots \mathbf{III.5}$$

III.3 Momentum Equation

The differential equation of the conservation of momentum in a given form is the derivation of Newton's second law.

However, there is a complication because both shear and normal stresses must be considered.

We write the corresponding momentum equation as (in x-direction):

$$\frac{\partial}{\partial t}(\rho u) + \operatorname{div}(\rho u u) = \operatorname{div}(u \operatorname{grad} u) - \frac{\partial P}{\partial x} + B_x + V_x \quad \ldots\ldots\ldots \text{III. 6}$$

where u is the viscosity, P is the pressure, Bx is the x-direction body force per unit volume, and Vx stands for the viscous terms that are in addition to those expressed by $div\ (u\ grad\ u)$. (34)

III.4 The General Differential Equation

If the dependent variable is symbolized by ϕ, the general differential equation is:

$$\frac{\partial}{\partial t}(\rho \phi) + \operatorname{div}(\rho u \phi) = \operatorname{div}(\Gamma \operatorname{grad} \phi) + S \quad \ldots\ldots\ldots \text{III. 7}$$

Where

- Γ is the diffusion coefficient
- S is the source term

The four terms of the differential equation include the unsteady term as well as the convection term, the term of diffusion and the source term.

The dependent variable (ϕ) represent variety of different quantities, such as the enthalpy or the temperature, a velocity component…; (34)

III.5 The Discretization Concept

The domain has been discretized: It is this systematic discretization of space and of the **dependent variables** that makes it possible to replace the governing differential equations with simple algebraic equations, which can be solved.

Discretization equation is an algebraic relation connecting the values of ϕ for a group of grid points.

The value of ϕ at a grid point influences the distribution of ϕ only in its immediate neighborhood.

As the number of grid points becomes very large, the solution of the discretization equations is expected to approach the exact solution of the corresponding differential equation, as the grid points get closer together, the change in between neighboring grid points becomes smaller.

Consider **Figure (III.1)** which shows a section of a discrete grid in the xy plane.

For convenience, let us assume that the spacing of the grid points in the x direction is uniform and given by Δx and that the spacing of the points in the y direction is also uniform and given by Δy **,**as shown in **Figure (III.1)**. In general, Δx and Δy are different.

We will assume uniform spacing in each coordinate direction but not necessarily equal spacing for both directions; i.e., we will assume Δx and Δy to be constants, but Δx does not have to equal Δy.

Returning to **Figure (III.1)**, the grid points are identified by an index i which runs in the x direction and an index j which runs in the y direction.

Hence, if (i, j) is the index for point **"P",** then the point immediately to the right of **"P"** is labeled as $(i + 1, j)$, the point immediately to the left is $(i - 1, j)$, the point directly above is $(i, j + 1)$, and the point directly below is $(i, j - 1)$. (33)

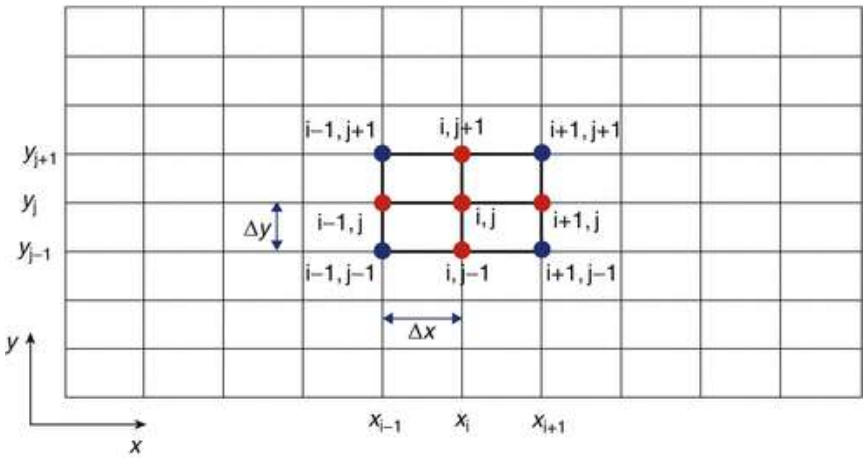

Figure III. 1- A section of a discrete grid in the xy plane.

III.5.1 Taylor-Series

The usual procedure for deriving finite-difference equations consists of approximating the derivatives in the differential equation via a Taylor series. (33)

Let us consider the grid points shown in **Figure (III.2)**.

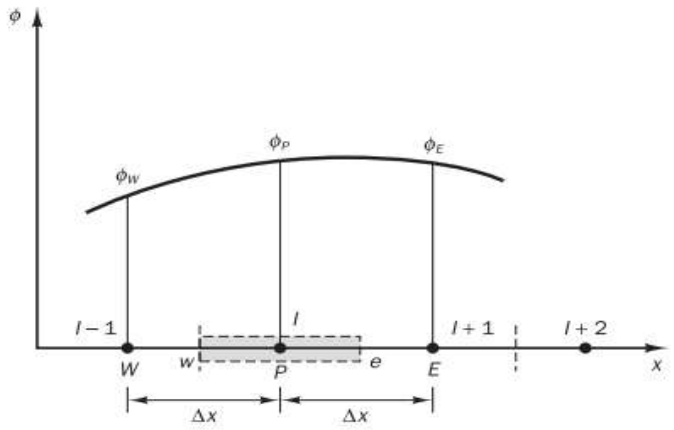

Figure III. 2-. A grid points

For a function $\phi(x)$ the Taylor series development of $\phi(x + \Delta x)$ around the point i at x is:

$$\boldsymbol{\phi(x + \Delta x) = \phi(x) + \Delta x\left(\frac{d\phi}{dx}\right)_x + \frac{1}{2}(\Delta x)^2\left(\frac{d^2\phi}{dx^2}\right)_x + \cdots \ldots \ldots \ldots \text{III. 8}}$$

In our notation we use discrete values ϕ_P and ϕ_E for $\phi(x)$ and $\phi(x + \Delta x)$ respectively so that previous equation can be written as:

$$\boldsymbol{\phi_E = \phi_P + \left(\frac{\partial\phi}{\partial x}\right)_P \Delta x + \left(\frac{\partial\phi^2}{\partial x^2}\right)_P \frac{\Delta x^2}{2} + \cdots \ldots \ldots \ldots \text{III. 8. a}}$$

$$\boldsymbol{\phi_w = \phi_P - \left(\frac{\partial\phi}{\partial x}\right)_P \Delta x + \left(\frac{\partial\phi^2}{\partial x^2}\right)_P \frac{\Delta x^2}{2} - \cdots \ldots \ldots \ldots \text{III. 8. b}}$$

This may be rearranged to give;

$$\left(\frac{\partial \phi}{\partial x}\right)_P = \frac{\phi_E - \phi_w}{2\Delta x} \dots\dots\dots \text{III. 9}$$

$$\left(\frac{\partial \phi^2}{\partial x^2}\right)_P = \frac{\phi_w + \phi_E - 2\phi_P}{(\Delta x)^2} \dots\dots\dots \text{III. 10}$$

In which:

- Γ represents the coefficient of diffusion.
- S is the source term.

Boundary values of ϕ at points A and B are defined.

A case study of this kind of process one-dimensional heat conduction within rods. (34)

III.6 Diffusion problem

Here we develop the numerical method based on this integration, the finite volume (or control volume) method, by considering the simplest transport process of all: **pure diffusion in the steady state.** (34)

The governing equation of steady diffusion can easily be derived from the general transport equation for property ϕ by deleting the transient and convective terms. This gives:

$$\mathbf{div}(\Gamma\, \mathbf{grad}\, \phi) + S_\phi = 0 \dots\dots\dots \text{III. 11}$$

Finite volume method for one dimensional steady state diffusion:

Consider the steady state diffusion of a property ϕ in a one-dimensional domain defined in **Figure (III.3)** The process is governed by:

$$\frac{d}{dx}\left(\Gamma\frac{d\phi}{dx}\right)+S=0 \ldots\ldots\ldots \text{III.11.}a$$

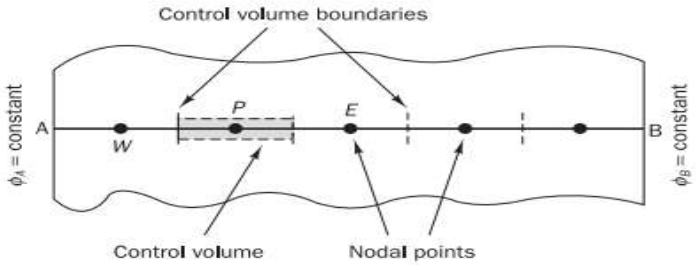

Figure III. 3- One-dimensional domain

- **Step 1: Grid generation**

The initial step of using the method of finite volumes is to divide the domain into discrete control volumes.

The boundaries (or faces) of control volumes are positioned mid-way between adjacent nodes. Thus, each node is surrounded by a control volume or cell. (34)

The usual convention of CFD methods is shown in **Figure (III.4).**

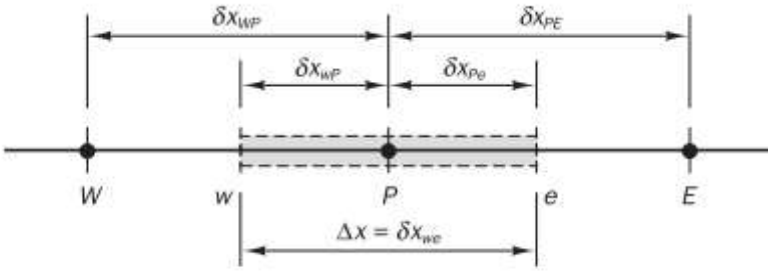

Figure III. 4- Convention of CFD methods

The general nodal point is "***P***", and its neighbors to the east and west are identified by W and E.

- **Step 2: Discretization**

The key step of the finite volume method is the integration of the governing equation (or equations) over a control volume to yield a discretized equation at its nodal point **P**.

For the control volume defined above this gives:

$$\int_{\Delta V} \frac{d}{dx}\left(\Gamma \frac{d\phi}{dx}\right) dV + \int_{\Delta V} S dV = \left(\Gamma A \frac{d\phi}{dx}\right)_c - \left(\Gamma A \frac{d\phi}{dx}\right)_w + \bar{S}\Delta V = 0 \quad \ldots\ldots\ldots \text{III. 11. b}$$

Here

- A is the cross-sectional area of the control volume face.
- ΔV is the volume.

$\bar{S}$ is the average value of source S over the control volume.

It is an attractive aspect with the Finite Volume Method that the discretized equation is able to provide an obvious physical interpretation.

In order to derive useful forms of the discretized equations, the interface diffusion coefficient Γ and the gradient $\frac{d\phi}{dx}$ at east (e) and west (w) are required.

Linear approximations seem to be the obvious and simplest way of calculating interface values and the gradients. (34)

This practice is called central differencing. In a uniform grid linearly interpolated values for Γ_w and Γ_e are given by:

$$\Gamma_w = \frac{\Gamma_W + \Gamma_p}{2} \quad \ldots\ldots\ldots \text{III. 12}$$

$$\Gamma_c = \frac{\Gamma_P + \Gamma_E}{2} \dots\dots\dots \text{III. 13}$$

And the diffusive flux terms are evaluated as:

$$\left(\Gamma A \frac{d\phi}{dx}\right)_e = \Gamma_\epsilon A_e \left(\frac{\phi_E - \phi_P}{\delta r_{PE}}\right) \dots\dots\dots \text{III. 14}$$

$$\left(\Gamma A \frac{d\phi}{dx}\right)_w = \Gamma_w A_W \left(\frac{\phi_P - \phi_W}{\delta x_{WP}}\right) \dots\dots\dots \text{III. 15}$$

The source term S is a function of the dependent variable. In some cases, the finite volume method approximates the source term by means of a linear form:

$$\bar{S}\Delta V = S_u + S_p\phi_P \dots\dots\dots \text{III. 16}$$

By the substitution of equations, we have:

$$\Gamma_c A_e \left(\frac{\phi_E - \phi_P}{\delta x_{PE}}\right) - \Gamma_w A_w \left(\frac{\phi_p - \phi_W}{\delta x_{WP}}\right) + \left(S_P + S_p\phi_P\right) = 0 \dots\dots\dots (\text{III. 17})$$

This can be rearranged as:

$$\left(\frac{\Gamma_c}{\delta x_{PE}} A_e + \frac{\Gamma_w}{\delta x_{WP}} A_w - S_p\right)\phi_P = \left(\frac{\Gamma_w}{\delta x_{WP}} A_w\right)\phi_W + \left(\frac{\Gamma_c}{\delta x_{PE}} A_e\right)\phi_E + S_u \dots\dots\dots \text{III. 17. a}$$

Identifying the coefficients of ϕ_W and ϕ_E in the previous equation as a_W and a_E , and the coefficient of ϕ_P as a_P , the above equation can be written as:

$$\mathbf{a_P\phi_p = a_W\phi_W + a_E\phi_E + S_u} \dots\dots\dots \mathbf{III.18}$$

Where:

Table III. 1

a_W	a_E	a_P
$\frac{\Gamma_w}{\delta_{x_{WP}}} A_w$	$\frac{\Gamma_e}{\delta x_{pE}} A_e$	$a_W + a_E - S_p$

- **Step 3: Solution of equations**

Discretized equations of the form $III.18$ must be set up at each of the nodal points in order to solve a problem.

The resulting system of linear algebraic equations is then solved to obtain the distribution of the property ϕ at nodal points.

The finite volume method for convection---diffusion problems.

In cases in which fluid flow plays an important role, we need to take into account the effects of convection.

It is common for diffusion to occur alongside convection in nature. Therefore, we look at methods to predict combined convection and diffusion.

The steady convection–diffusion equation can be derived from the transport equation for a general property ϕ by deleting the transient term:

$$\mathbf{div}(\boldsymbol{\rho u \phi}) = \mathbf{div}(\boldsymbol{\Gamma}\ \mathbf{grad}\ \boldsymbol{\phi}) + \mathbf{S_{\phi}} \ldots\ldots\ldots \mathbf{III.19}$$

This equation represents the flux balance in a control volume. The left-hand side gives the net convective flux and the right-hand side contains the net diffusive flux. (34)

In the absence of sources, steady convection and diffusion of a property ϕ in a given one-dimensional flow field u is governed by:

$$\frac{\mathbf{d}}{\mathbf{dx}}(\boldsymbol{\rho u \phi}) = \frac{\mathbf{d}}{\mathbf{dx}}\left(\boldsymbol{\Gamma}\frac{\mathbf{d}\boldsymbol{\phi}}{\mathbf{dx}}\right) \ldots\ldots\ldots \mathbf{III.20}$$

The flow must also satisfy continuity, so:

$$\frac{\mathbf{d}(\boldsymbol{\rho u})}{\mathbf{dx}} = \mathbf{0} \ldots\ldots\ldots \mathbf{III.21}$$

We consider the one-dimensional control volume shown in **Figure III.5**

Integration of transport equation (5.3) over the control volume of **Figure III.5** gives:

$$(\boldsymbol{\rho u A \phi})_{\mathbf{e}} - (\boldsymbol{\rho u A \phi})_{\mathbf{w}} = \left(\boldsymbol{\Gamma A}\frac{\mathbf{d}\boldsymbol{\phi}}{\mathbf{dx}}\right)_{\mathbf{e}} - \left(\boldsymbol{\Gamma A}\frac{\mathbf{d}\boldsymbol{\phi}}{\mathbf{dx}}\right)_{\mathbf{w}} \ldots\ldots\ldots \mathbf{III.20.a}$$

And integration of continuity equation $III.21$ yields:

$$(\boldsymbol{\rho u A})_{\mathbf{e}} - (\boldsymbol{\rho u A})_{\mathbf{w}} = \mathbf{0} \ldots\ldots\ldots \mathbf{III.21.a}$$

It is convenient to define two variables F and D to represent the convective mass flux per unit area and diffusion conductance at cell faces, to obtain discretized equationsfor the convection–diffusion problem we must approximate the terms in equation $III.20.a$:

$$\mathbf{F} = \boldsymbol{\rho u} \ldots\ldots\ldots \mathbf{III.22}$$

$$\mathbf{D = \frac{\Gamma}{\delta x} \dots \dots \dots III.23}$$

The variables F and D (in faces) can be written as:

$$\mathbf{F_w = (\rho u)_w \quad F_e = (\rho u)_e \dots \dots \dots III.24}$$

$$\mathbf{D_w = \frac{\Gamma_w}{\delta x_{WP}} \quad D_e = \frac{\Gamma_e}{\delta x_{PE}} \dots \dots \dots III.25}$$

Assuming that $A_w = A_e = A$, so we can divide the left- and right-hand sides of equation $III.20.a$ by area A.

Like before, we use the central differencing method to represent the contribution of the diffusion terms on the right-hand side. (34)

The integrated convection–diffusion equation $III.20.a$ can now be written as:

$$\mathbf{F_e\phi_e - F_w\phi_w = D_e(\phi_E - \phi_P) - D_w(\phi_P - \phi_W) \dots \dots \dots III.26}$$

In order to solve equation $III.26$ we need to calculate the transported property ϕ at the e and w faces.

Schemes for this purpose are assessed in the **following sections**.

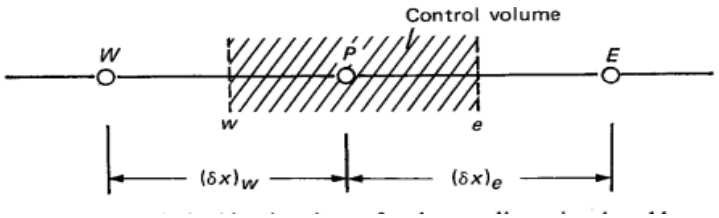

Figure III. 5- control volume

III.7 Schemes

III.7.1 The central differencing scheme

The central differencing approximation has been used to represent the diffusion terms which appear on the right-hand side of the equation. and it seems logical to try linear interpolation to compute the cell face values for the convective terms on the left-hand side of this equation. (35)

For a uniform grid we can write the cell face values of property ϕ as:

$$\phi_e = \frac{(\phi_P + \phi_E)}{2} \dots\dots\dots \text{III.27}$$

$$\phi_w = \frac{(\phi_W + \phi_P)}{2} \dots\dots\dots \text{III.28}$$

Substitution of the above expressions into the convection terms of $III.26$ yields

$$\frac{F_e}{2}(\phi_P + \phi_E) - \frac{F_w}{2}(\phi_W + \phi_P) = D_e(\phi_E - \phi_P) - D_w(\phi_P - \phi_W) \dots\dots\dots \text{III.29}$$

This can be rearranged to give

$$\left[\left(D_w - \frac{F_w}{2}\right) + \left(D_e + \frac{F_e}{2}\right)\right]\phi_P = \left(D_w + \frac{F_w}{2}\right)\phi_W + \left(D_e - \frac{F_e}{2}\right)\phi_E$$

$$\left[\left(D_w + \frac{F_w}{2}\right) + \left(D_e - \frac{F_e}{2}\right) + (F_e - F_w)\right]\phi_P = \left(D_w + \frac{F_w}{2}\right)\phi_W + \left(D_e - \frac{F_e}{2}\right)\phi_E \dots\dots\dots \text{III.30}$$

Identifying the coefficients of ϕ_W and ϕ_E as a_W and a_E , the central differencing expressions for the discretized convection–diffusion equation are:

$$a_P\phi_P = a_W\phi_W + a_E\phi_E \dots\dots\dots \text{III.31}$$

Where:

Table III. 2

a_W	a_E	a_P
$D_w + \frac{F_w}{2}$	$D_e - \frac{F_e}{2}$	$a_W + a_E + (F_e - F_w)$

To solve a one-dimensional convection–diffusion problem we write discretized equations of the form $III.31$ for all grid nodes.

This yields a set of algebraic equations that is solved to obtain the distribution of the transported property ϕ.

III.7.2 The upwind differencing schemes

One of the major problems of the central differencing scheme is its inability to identify flow direction.

The value of property ϕ at a west cell face is always influenced by both ϕ_P and ϕ_W in central differencing. In a strongly convective flow from west to east, the above treatment is unsuitable because the west cell face should receive much stronger influence from node W than from node P. (34)

The **upwind differencing** or **'donor cell'** differencing scheme takes into account the flow direction when determining the value at a cell face: the convicted value of ϕ at a cell face is taken to be equal to the value at the upstream node.

In **Figure (III.6)** we show the nodal values used to calculate cell face values when the flow is in the positive direction (west to east) and in **Figure (III.7)** those for the negative direction.

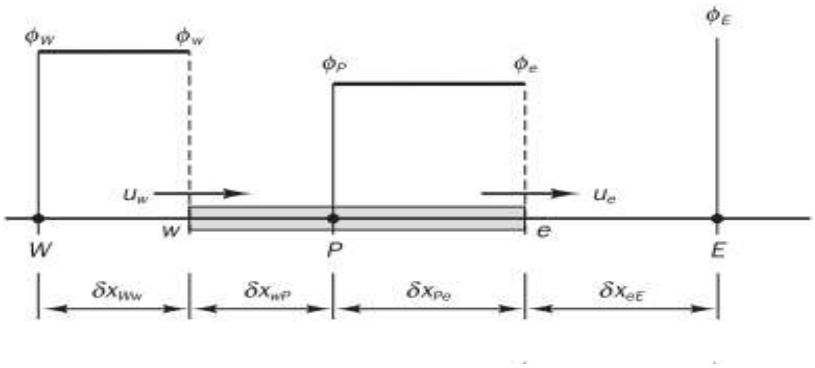

Figure III. 6- the nodal values used to calculate cell face values when the flow is in the positive direction.

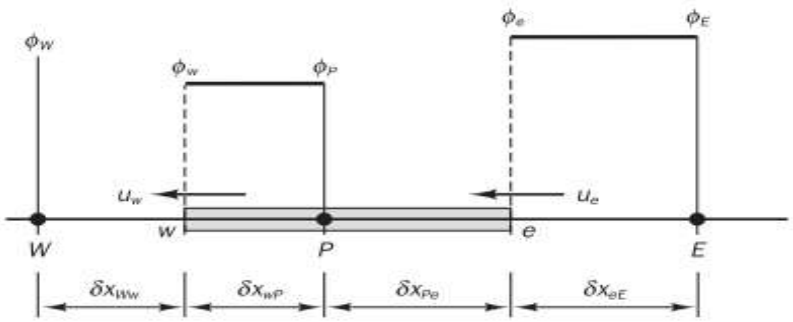

Figure III. 7-the nodal values used to calculate cell face values when the flow is in the negative direction.

When the flow is in the positive direction, $u_w > 0, u_e > 0$ ($F_w > 0, F_e > 0$), the upwind scheme sets:

$$\boldsymbol{\phi_w = \phi_W \text{ and } \phi_e = \phi_P} \ldots\ldots\ldots \textbf{III. 32}$$

And the discretized equation $III.26$ becomes:

$$\boldsymbol{F_e\phi_P - F_w\phi_W = D_e(\phi_E - \phi_P) - D_w(\phi_P - \phi_W)} \ldots\ldots\ldots \textbf{III. 33}$$

Which can be rearranged as

$$\boldsymbol{(D_w + D_e + F_e)\phi_P = (D_w + F_w)\phi_W + D_e\phi_E} \ldots\ldots\ldots \textbf{III. 34}$$

To give:

$$[(\mathbf{D_w} + \mathbf{F_w}) + \mathbf{D_e} + (\mathbf{F_e} - \mathbf{F_w})]\boldsymbol{\phi}_\mathbf{P} = (\mathbf{D_w} + \mathbf{F_w})\boldsymbol{\phi}_\mathbf{W} + \mathbf{D_e}\boldsymbol{\phi}_\mathbf{E} \dots\dots\dots \mathbf{III.35}$$

When the flow is in the negative direction, $u_w < 0, u_e < 0$ ($F_w < 0, F_e < 0$), the scheme takes

$$\boldsymbol{\phi}_\mathbf{w} = \boldsymbol{\phi}_\mathbf{P} \textbf{ and } \boldsymbol{\phi}_\mathbf{e} = \boldsymbol{\phi}_\mathbf{E} \dots\dots\dots \mathbf{III.36}$$

Now the discretized equation is :

$$\mathbf{F_e}\boldsymbol{\phi}_\mathbf{E} - \mathbf{F_w}\boldsymbol{\phi}_\mathbf{P} = \mathbf{D_e}(\boldsymbol{\phi}_\mathbf{E} - \boldsymbol{\phi}_\mathbf{P}) - \mathbf{D_w}(\boldsymbol{\phi}_\mathbf{P} - \boldsymbol{\phi}_\mathbf{W}) \dots\dots\dots \mathbf{III.37}$$

Or

$$[\mathbf{D_w} + (\mathbf{D_e} - \mathbf{F_e}) + (\mathbf{F_e} - \mathbf{F_w})]\boldsymbol{\phi}_\mathbf{P} = \mathbf{D_m}\boldsymbol{\phi}_\mathbf{W} + (\mathbf{D_e} - \mathbf{F_e})\boldsymbol{\phi}_\mathbf{E} \dots\dots\dots \mathbf{III.38}$$

Identifying the coefficients of ϕ_E and ϕ_W as a_E and a_W , equations $III.35$ and $\boldsymbol{III.38}$ can be written in the usual general form:

$$\mathbf{a_P}\boldsymbol{\phi}_\mathbf{P} = \mathbf{a_W}\boldsymbol{\phi}_\mathbf{W} + \mathbf{a_E}\boldsymbol{\phi}_\mathbf{E} \dots\dots\dots \mathbf{III.39}$$

With central coefficient:

$$\mathbf{a_P} = \mathbf{a_W} + \mathbf{a_E} + (\mathbf{F_e} - \mathbf{F_w}) \dots\dots\dots \mathbf{III.40}$$

And neighbor's coefficients

Table III. 3

	a_W	a_E
$F_w > 0, F_e > 0$	$D_w + F_w$	D_e
$F_w < 0, F_e < 0$	D_w	$D_e - F_e$

Form of notation for the neighbor coefficients of the upwind differencing method that covers both flow directions is given below:

Table III. 4

a_W	a_E
$D_w + max(F_w, 0)$	$D_e + max(0, -F_e)$

III.8 QUICK scheme

The accuracy of upwind scheme is only first-order. The use of upwind quantities ensures that the schemes are very stable, but the first-order accuracy makes them prone to numerical diffusion errors.

Such errors can be minimized by employing higher-order discretization. Higher-order schemes involve more neighbor points and reduce the discretization errors by bringing in a wider influence.

The central differencing scheme, which has second-order accuracy, proved to be unstable, formulations that do not take into account the flow direction are unstable

and, therefore, more accurate higher order schemes, which preserve upwind scheme for stability and sensitivity to the flow direction, are needed. (34)

The quick scheme uses a three-point, quadratic interpolation for cell face values. The face value of ϕ is obtained from a quadratic function passing through two bracketing nodes (on each side of the face) and a node on the upstream side **(Figure III.8).**

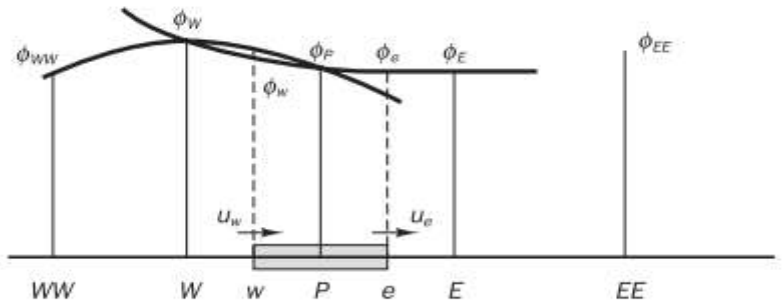

Figure III. 8- the nodal values used to calculate cell face values when the flow is in the positive direction.

For example, when $u_w > 0$ and $u_e > 0$. A quadratic fit through WW, W and P is used to evaluate ϕ_w, and a further quadratic fit through W, P and E to calculate ϕ_e .

For $u_w < 0$ and $u_e < 0$ values of ϕ at W, P and E are used for ϕ_w, and values at P, E and EE for ϕ_e .

It can be shown that for a uniform grid the value of ϕ at the cell face between two bracketing nodes i and $i - 1$ and upstream node $i - 2$ is given by the following formula:

$$\boldsymbol{\phi_{face} = \frac{6}{8}\phi_{i-1} + \frac{3}{8}\phi_i - \frac{1}{8}\phi_{i-2} \dots\dots\dots \text{III. 41}}$$

When $u_w > 0$, the bracketing nodes for the west face w are W and P, the upstream node is WW **(Figure III.8)**

$$\phi_w = \frac{6}{8}\phi_W + \frac{3}{8}\phi_P - \frac{1}{8}\phi_{WW} \dots\dots\dots \mathbf{III.41}$$

When $u_e > 0$, the bracketing nodes for the east face e are P and E, the upstream node is W, so:

$$\phi_e = \frac{6}{8}\phi_P + \frac{3}{8}\phi_E - \frac{1}{8}\phi_W \dots\dots\dots \mathbf{III.42}$$

The diffusion terms may be evaluated using the gradient of the approximating parabola.

It is interesting to note that on a uniform grid this practice gives the same expressions as central differencing for diffusion, since the slope of the chord between two points on a parabola is equal to the slope of the tangent to the parabola at its midpoint.

If $F_w > 0$ and $F_e > 0$, and if we use equations $\boldsymbol{III.41}$ – $III.42$ for the convective terms and central differencing for the diffusion terms, the discretized form of the one-dimensional convection– diffusion transport equation $III.26$ may be written as

$$\left[F_e\left(\frac{6}{8}\phi_P + \frac{3}{8}\phi_E - \frac{1}{8}\phi_W\right) - F_w\left(\frac{6}{8}\phi_W + \frac{3}{8}\phi_P - \frac{1}{8}\phi_{WW}\right)\right] = D_e(\phi_E - \phi_P) - D_m(\phi_P - \phi_W) \dots\dots\dots \mathbf{III.43}$$

Which can be rearranged to give

$$\left[D_w - \frac{3}{8}F_w + D_c + \frac{6}{8}F_c\right]\phi_P = \left[D_w + \frac{6}{8}F_w + \frac{1}{8}F_c\right]\phi_W + \left[D_c - \frac{3}{8}F_c\right]\phi_E - \frac{1}{8}F_w\phi_{WW} \dots\dots\dots III.44$$

This is now written in the standard form for discretized equations:

$$\mathbf{a_P\phi_P = a_W\phi_W + a_E\phi_E + a_{WW}\phi_{WW} \dots\dots\dots III.45}$$

Where:

Table III. 5

a_W	a_E	a_{WW}	a_p
$D_w + \frac{6}{8}F_w + \frac{1}{8}F_e$	$D_e - \frac{3}{8}F_e$	$-\frac{1}{8}F_w$	$a_W + a_E + a_{WW} + (F_e - F_w)$

For $Fw < 0$ and $Fe < 0$ the flux across the west and east boundaries is given by the expressions:

$$\mathbf{\phi_w = \frac{6}{8}\phi_P + \frac{3}{8}\phi_W - \frac{1}{8}\phi_E \dots\dots\dots III.46}$$

$$\mathbf{\phi_e = \frac{6}{8}\phi_E + \frac{3}{8}\phi_P - \frac{1}{8}\phi_{EE} \dots\dots\dots III.47}$$

Substitution of these two formulae for the convective terms in the discretized convection–diffusion equation $III.26$ together with central differencing for the diffusion terms leads, after rearrangement as above, to the following coefficients:

Table III. 6

a_W	a_E	a_{EE}	a_P
$D_w + \frac{3}{8}F_w$	$D_e - \frac{6}{8}F_e - \frac{1}{8}F_w$	$\frac{1}{8}F_e$	$a_W + a_E + a_{EE} + (F_e - F_w)$

General expressions, valid for positive and negative flow directions, can be obtained by combining the two sets of coefficients above.

The quick scheme for one-dimensional convection–diffusion problems can be summarized as follows:

$$\mathbf{a_P\phi_P = a_W\phi_W + a_E\phi_E + a_{WW}\phi_{WW} + a_{EE}\phi_{EE} \dots\dots\dots III.48}$$

With central coefficient:

$$\mathbf{a_P = a_W + a_E + a_{WW} + a_{EE} + (F_e - F_w) \dots\dots\dots III.49}$$

And neighbor coefficients:

Table III. 7

a_W	a_{WW}	a_E	a_{EE}
$D_w + \frac{6}{8}\alpha_w F_w + \frac{1}{8}\alpha_e F$ $+\frac{3}{8}(1-\alpha_w)F_w$	$-\frac{1}{8}\alpha_w F_w$	$D_e - \frac{3}{8}\alpha_e F_e - \frac{6}{8}(1-\alpha_e)$ $-\frac{1}{8}(1-\alpha_w)F_w$	$\frac{1}{8}(1-\alpha_e)F_e$

Where

$\boldsymbol{\alpha_w = 1}$ **for** $\boldsymbol{F_w > 0}$ **and** $\boldsymbol{\alpha_e = 1}$ **for** $\boldsymbol{F_e > 0}$

$\boldsymbol{\alpha_w = 0}$ **for** $\boldsymbol{F_w < 0}$ **and** $\boldsymbol{\alpha_e = 0}$ **for** $\boldsymbol{F_e < 0}$

III.8.1 The quick scheme: stability problems of and remedies:

Since the QUICK scheme in the form presented above can be unstable due to the appearance of negative main coefficients, it has been reformulated in different ways that alleviate stability problems.

These formulations all involve placing troublesome negative coefficients in the source term so as to retain positive main coefficients. The contributing part is appropriately weighted to give better stability and positive coefficients as far as possible. (34)

The approach below for rearranging QUICK schemes and derived a stable and fast converging variant, this approach can be summarized as follow.

$$\phi_w = \phi_W + \frac{1}{8}[3\phi_P - 2\phi_W - \phi_{WW}] \text{ / for } F_w > 0 \dots\dots\dots \text{III. 50}$$

$$\phi_e = \phi_P + \frac{1}{8}[3\phi_E - 2\phi_P - \phi_W] \text{ / for } F_e > 0 \dots\dots\dots \text{III. 51}$$

$$\phi_w = \phi_P + \frac{1}{8}[3\phi_W - 2\phi_P - \phi_E] \text{ / for } F_w < 0 \dots\dots\dots \text{III. 52}$$

$$\phi_e = \phi_E + \frac{1}{8}[3\phi_P - 2\phi_E - \phi_{EE}] \text{ / for } F_e < 0 \dots\dots\dots \text{III. 53}$$

The discretization equation takes the general form as usual:

$$a_P\phi_P = a_W\phi_W + a_E\phi_E + \bar{S} \dots\dots\dots \text{III. 54}$$

The main coefficient is :

$$a_P = a_W + a_E + (F_e - F_w) \dots\dots\dots \text{III. 55}$$

Table III. 8

a_W	a_E	$\overline{S}$
$D_w + \alpha_w F_w$	$D_e - (1-\alpha_e)F_e$	$\frac{1}{8}(3\phi_P - 2\phi_W - \phi_{WW})\alpha_w F_w + \frac{1}{8}(\phi_W + 2\phi_P - 3\phi_E)\alpha_e F_e + \frac{1}{8}(3\phi_W - 2\phi_P - \phi_E)(1-\alpha_w)F_w + \frac{1}{8}(2\phi_E + \phi_{EE} - 3\phi_P)(1-\alpha_e)F_e$

Where

$$\alpha_w = 1 \text{ for } F_w > 0 \text{ and } \alpha_e = 1 / \text{ for } F_e > 0$$

$$\alpha_w = 0 \text{ for } F_w < 0 \text{ and } \alpha_e = 0 \text{ for } F_e < 0$$

The advantage of this approach is that the main coefficients are positive.

III.8.2 The accuracy of the QUICK scheme

The QUICK differencing scheme has greater formal accuracy than the central differencing. **(Figure III.9)** shows a comparison between upwind and QUICK for the two-dimensional test. (33)

It can be seen that the QUICK scheme matches the exact solution much more accurately than the upwind scheme on a 50 × 50 grid. weighted to give better stability and positive coefficients as far as possible. (34)

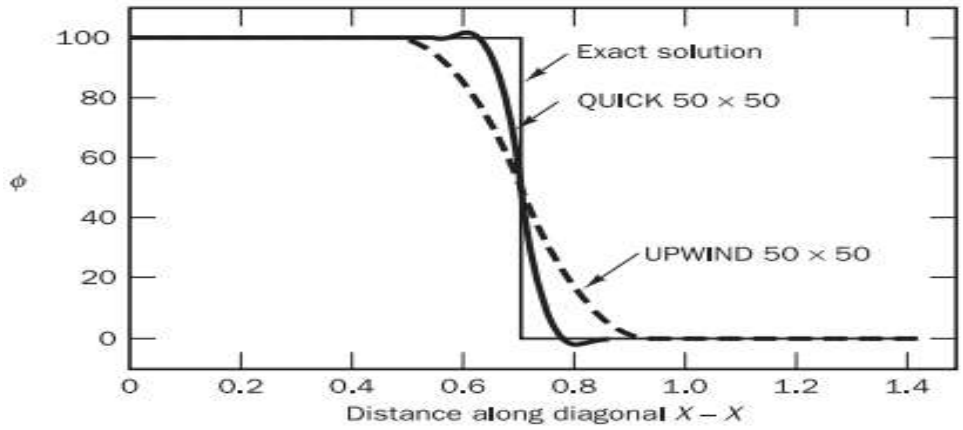

Figure III. 9- A comparison between quick, upwind and exact solution

The quick scheme can, however, give undershoots and overshoots, as is evident in **Figure III.9.**

The possibility of undershoots and overshoots needs to be considered when interpreting solutions.

We will use **QUICK scheme** in our simulation for more accuracy.

III.8.3 Quick summary

We have discussed the problems of discretizing the convection–diffusion equation under the assumption that the flow field is known.

The crucial issue is the formulation of suitable expressions for the values of the transported property ϕ at cell faces when accounting for the convective contribution in the equation:

All the finite volume schemes presented in this chapter describe the effects of simultaneous convection and diffusion by means of discretized equations whose coefficients are weighted combinations of the convective mass flux per unit area $\boldsymbol{F}$ and the diffusion conductance $\boldsymbol{D}$. weighted to give better stability and positive coefficients as far as possible. (34)

- **T**he discretized equations for a general internal node for the central, upwind and quick schemes of a one-dimensional convection–diffusion problem take the following form:

$$\mathbf{a_P\phi_P = a_W\phi_W + a_E\phi_E} \dots\dots\dots \mathbf{III.56}$$

With:

$$\mathbf{a_P = a_W + a_E + (F_e - F_w)} \dots\dots\dots \mathbf{III.57}$$

• The neighbour coefficients for these schemes are:

Table III. 9

	a_E	a_W
Central differencing	$D_e - F_e/2$	$D_w + F_w/2$
Upwind	$D_e + max(0, -F_e)$	$D_w + max(F_w, 0)$

The discretized equations of the standard QUICK method of Leonard (1979) have the following form for a general internal node point:

$$\mathbf{a_P\phi_P = a_W\phi_W + a_E\phi_E + a_{WW}\phi_{WW} + a_{EE}\phi_{EE}} \dots\dots\dots \mathbf{III.58}$$

Where

$$\mathbf{a_P = a_W + a_E + a_{WW} + a_{EE} + (F_e - F_w)} \dots\dots\dots \mathbf{III.59}$$

QUICK:
$$a_W = D_w + \frac{6}{8}\alpha_w F_w + \frac{1}{8}\alpha_e F_e + \frac{3}{8}(1-\alpha_w)F_w$$
$$a_{WW} = -\frac{1}{8}\alpha_w F_w$$
$$a_E = D_e - \frac{3}{8}\alpha_e F_e - \frac{6}{8}(1-\alpha_e)F_e - \frac{1}{8}(1-\alpha_w)F_w$$
$$a_{EE} = \frac{1}{8}(1-\alpha_e)F_e$$

With:

$$\alpha_w = 1 \text{ for } F_w > 0 \text{ and } \alpha_e = 1 \text{ for } F_e > 0$$

$$\alpha_m = 0 \text{ for } F_m < 0 \text{ and } \alpha_e = 0 \text{ for } F_e < 0$$

III.9 WRAPS-UP

Higher-order schemes, such as **QUICK (what we will use in our simulation)**, can be less computationally stable.

This manifests itself as small over- and undershoots in the solution of some problems including those with large gradients of ϕ, which can potentially lead to non-physical behavior

Nevertheless, if used with care and judgement the **QUICK** scheme can give very accurate solutions of convection–diffusion problems.

III.10 Solution algorithms for pressure---velocity coupling in steady flows

The convection of a scalar variable ϕ depends on the magnitude and direction of the local velocity field. We assumed that the velocity field was somehow known.

In general, the velocity field is, however, not known and emerges as part of the overall solution process along with all other flow variables.

Transport equations for each velocity component – momentum equations – can be derived from the general transport equation by replacing the variable ϕ by u, v and w respectively. (35)

Every velocity component appears in each momentum equation, and the velocity field must also satisfy the continuity equation. This can be clearly shown by considering the equations governing a two-dimensional laminar steady flow:

- ✓ **x-momentum equation:**

$$\frac{\partial}{\partial x}(\rho u u) + \frac{\partial}{\partial y}(\rho v u) = \frac{\partial}{\partial x}\left(\mu \frac{\partial u}{\partial x}\right) + \frac{\partial}{\partial y}\left(\mu \frac{\partial u}{\partial y}\right) - \frac{\partial p}{\partial x} + S_u \quad \ldots\ldots\ldots \text{III. 60}$$

- ✓ **y-momentum equation:**

$$\frac{\partial}{\partial x}(\rho u v) + \frac{\partial}{\partial y}(\rho v v) = \frac{\partial}{\partial x}\left(\mu \frac{\partial v}{\partial x}\right) + \frac{\partial}{\partial y}\left(\mu \frac{\partial v}{\partial y}\right) - \frac{\partial p}{\partial y} + S_v \quad \ldots\ldots\ldots \text{III. 61}$$

- ✓ **continuity equation:**

$$\frac{\partial}{\partial x}(\rho u) + \frac{\partial}{\partial y}(\rho v) = 0 \quad \ldots\ldots\ldots \text{III. 62}$$

The solution of equation set $III.60$– $III.62$ presents us with two new problems:

- The convective terms of the momentum equations contain non-linear quantities: for example, the first term of equation $III.60$ is the x-derivative of ρu^2.
- All three equations are intricately coupled because every velocity component appears in each momentum equation and in the continuity equation.
- The most complex issue to resolve is the role played by the pressure. It appears in both momentum equations, but there is evidently no (transport or other) equation for the pressure.
- If the pressure gradient is known, the process of obtaining discretized equations for velocities from the momentum equations is exactly the same as that for any other scalar, and the schemes explained are applicable.

III.11 The momentum equations

As mentioned earlier, if the pressure field is known, the discretization of velocity equations and the subsequent solution procedure is the same as that of a scalar equation. Since the velocity grid is staggered the new notation based on grid line and cell face numbering will be used.

In (**Figure III.10)** the unbroken grid lines are numbered by means of capital letters. In the x-direction the numbering is $\ldots, I-1, I, I+1, \ldots$ etc. In the y-direction $\ldots, J-1, J, J+1, \ldots$ etc.

The dashed lines that construct the cell faces are denoted by lower case letters. $\ldots, i-1, i, i+1, \ldots and \ldots, j-1, j, j+1, \ldots$ in the x- and y-directions respectively.

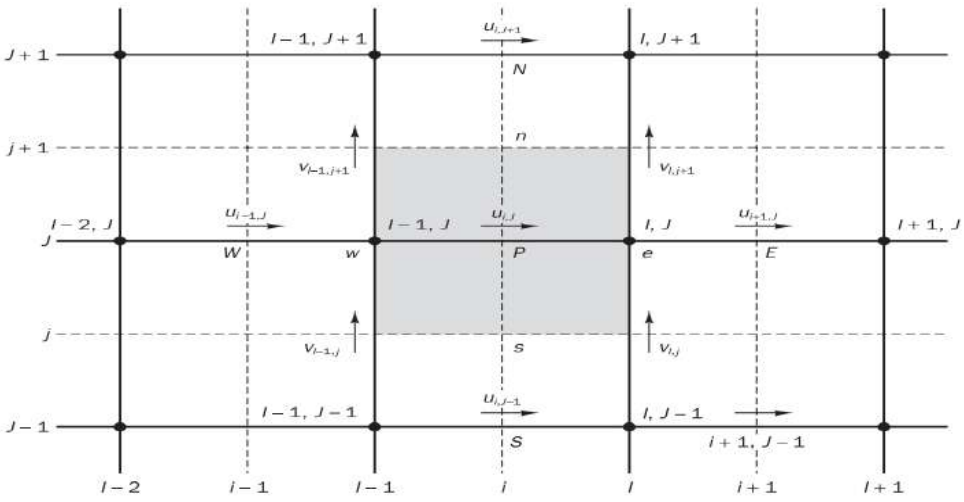

Figure III. 10- A grid board

The values of coefficients $a_{i,J}$ and a_{nb} may be calculated with any of the differencing methods (upwind, QUICK….) suitable for convection–diffusion problems.

The coefficients contain combinations of the convective flux per unit mass F and the diffusive conductance D at u-control volume cell faces. Applying the new notation system, we give the values of F and D for each of the faces e, w, n *and* s of the u-control volume:

$$\mathbf{F_w = (\rho u)_w = \frac{F_{i,J} + F_{i-1,J}}{2}} \\ \mathbf{= \frac{1}{2}\left[\left(\frac{\rho_{I,J} + \rho_{I-1,J}}{2}\right) u_{i,J} + \left(\frac{\rho_{I-1,J} + \rho_{I-2,J}}{2}\right) u_{i-1,J}\right]} \quad \dots\dots\dots \mathbf{III.65.a}$$

$$\mathbf{F_e = (\rho u)_e = \frac{F_{i+1,J} + F_{i,J}}{2}} \\ \mathbf{= \frac{1}{2}\left[\left(\frac{\rho_{I+1,J} + \rho_{I,J}}{2}\right) u_{i+1,J} + \left(\frac{\rho_{I,J} + \rho_{I-1,\mathcal{J}}}{2}\right) u_{i,J}\right]} \quad \dots\dots\dots \mathbf{III.65.b}$$

$$F_s = (\rho v)_s = \frac{F_{I,j} + F_{I-1,j}}{2} = \frac{1}{2}\left[\left(\frac{\rho_{I,J} + \rho_{I,J-1}}{2}\right)v_{I,j} + \left(\frac{\rho_{I-1,J} + \rho_{I-1,J-1}}{2}\right)v_{I-1,j}\right] \quad \ldots\ldots\ldots \text{III. 65. c}$$

$$F_n = (\rho v)_n = \frac{F_{I,j+1} + F_{I-1,j+1}}{2} = \frac{1}{2}\left[\left(\frac{\rho_{I,J+1} + \rho_{I,J}}{2}\right)v_{I,j+1} + \left(\frac{\rho_{I-1,J+1} + \rho_{I-1,J}}{2}\right)v_{I-1,j+1}\right] \quad \ldots\ldots\ldots \text{III. 65. d}$$

$$D_w = \frac{\Gamma_{I-1,J}}{x_i - x_{i-1}} \quad \ldots\ldots\ldots \text{III. 65. e}$$

$$D_e = \frac{\Gamma_{I,J}}{x_{i+1} - x_i} \quad \ldots\ldots\ldots \text{III. 65. f}$$

$$D_s = \frac{\Gamma_{I-1,J} + \Gamma_{I,J} + \Gamma_{I-1,J-1} + \Gamma_{I,J-1}}{4(y_J - y_{J-1})} \quad \ldots\ldots\ldots \text{III. 65. g}$$

$$D_n = \frac{\Gamma_{I-1,J+1} + \Gamma_{I,J+1} + \Gamma_{I-1,J} + \Gamma_{I,J}}{4(y_{J+1} - y_J)} \quad \ldots\ldots\ldots \text{III. 65. h}$$

During each iteration the $u-$ and $v-$velocity components used to evaluate the above expressions are those obtained as the outcome of the previous iteration (or the initial guess in the first iteration).

By analogy the v −momentum equation becomes

$$\mathbf{a_{I,j}v_{I,j}} = \sum \mathbf{a_{nb}v_{nb}} + \mathbf{(p_{I,J-1} - p_{I,J})A_{I,j}} + \mathbf{b_{I,j}} \dots\dots\dots \mathbf{III.66}$$

The neighbors involved in the summation $\sum a_{nb} v_{nb}$ and prevailing velocities are as shown in (**Figure III.12).**

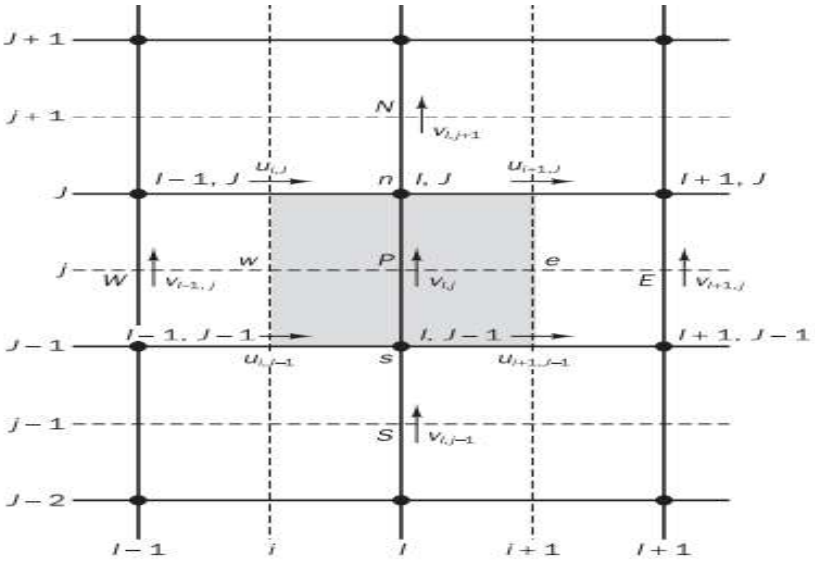

Figure.III.12. A second grid board

Coefficients $a_{I,j}$ and a_{nb} again contain combinations of the convective flux per unit mass F and the diffusive conductance D at v −control volume cell faces. Their values are obtained by the same averaging procedure adopted for the u −control volume.

Again, at each iteration level the values of F are computed using the $u-$ and $v-$ velocity components resulting from the previous iteration.

Given a pressure field **P**, discretized momentum equations can be written for each $u-$ and v −control volume and then solved to obtain the velocity fields.

If the pressure field is correct the resulting velocity field will satisfy continuity. As the pressure field is unknown, we need a method for calculating pressure. weighted to give better stability and positive coefficients as far as possible. (34)

III.12 Simple method

The SIMPLE algorithm gives a method of calculating pressure and velocities. The method is iterative, and when other scalars are coupled to the momentum equations the calculation needs to be done sequentially. weighted to give better stability and positive coefficients as far as possible. (34)

The sequence of operations in a CFD procedure which employs the simple algorithm given in (**Figure III.11).**

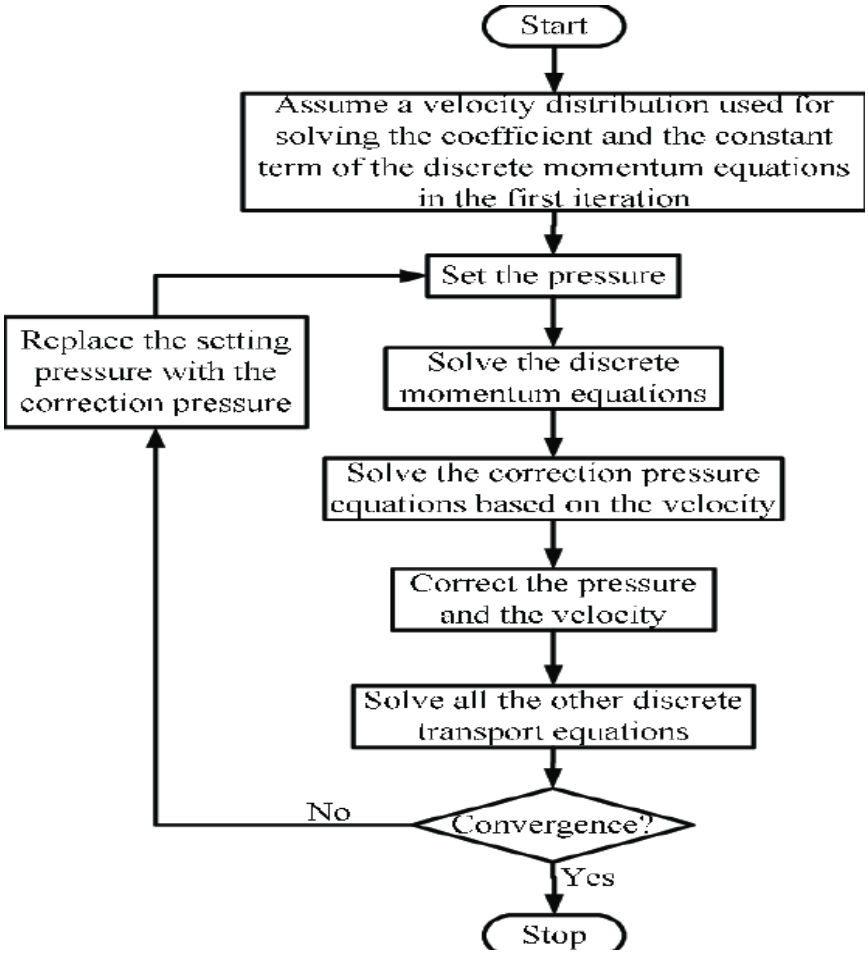

Figure III. 11-A summary of simple algo process. (32)

III.13 Conclusion

Previously, we have discussed methods of discretizing the governing equations of fluid flow This process results in a system of linear algebraic equations which needs to be solved.

The complexity and size of the set of equations depends on the dimensionality of the problem, the number of grid nodes and the discretization practice. Although any valid procedure can be used to solve the algebraic equations, the available computer resources set a powerful constraint.

There are two families of solution techniques for linear algebraic equations: direct methods and indirect or iterative methods. Simple examples of direct methods are Cramer's rule matrix inversion and Gaussian elimination.

Iterative methods are based on the repeated application of a relatively simple algorithm leading to eventual convergence after a – sometimes large – number of repetitions. Well-known examples are the Jacobi and Gauss– Seidel point-iterative methods.

Stronger still, it is not possible to guarantee convergence unless the system of equations satisfies fairly exacting criteria.

The finite volume method usually yields systems of equations. Since the systems arising from realistic CFD problems can be very large – up to 100 000 to 1 million equations – we find that iterative methods are generally much more economical than direct methods.

Thomas (1949) developed a technique for rapidly solving tri-diagonal systems that is now called the Thomas algorithm or the tri-diagonal matrix algorithm (TDMA). The TDMA is actually a direct method for one dimensional situation, but it can be applied iteratively, in a line-by-line fashion, to solve multi-dimensional problems and is widely used in CFD programs.

CHAPTRE

IV

CFD ANALYSIS

IV. CFD ANALYSIS

IV.1 Introduction

Drilling fluids have become more and more complex to meet the different needs of drilling operations. Accurate prediction of frictional pressure losses during drilling is complicated due to the combination of different drilling parameters.

In our study, computational fluid dynamics (CFD) analysis was performed to investigate the hydraulics of a solid-free non-Newtonian drilling fluid with an eccentric annulus coupled with a rotating drill string.

The **Herschel-Bulkley** fluid model is used to describe the non-Newtonian fluid behavior of drilling fluids. The fluid velocity at the annular inlet varies from $0.5\ to\ 1.2\ m/s$ (laminar flow).

Simulation results were compared with experimental data from internal flow loop results **(the experimental results were taking from this thesis)** (36). The flow circuit has a $10\ m$ long annular section with a $100\ mm$ inner diameter (ID) wellbore and a $50\ mm$ outer diameter (OD) fully eccentric drill string.

The pressure drop predictions from the CFD analysis are in close agreement with the experimental results.

From the test results, it can be seen that drilling fluids with similar viscosity distributions and densities exhibit different pressure drops. This work will contribute to a better understanding of the hydraulic behavior of drilling fluids.

IV.2 Geometry and Drilling-Fluids Specifications

The annulus between the drill pipe and the wellbore or casing is denoted as concentric and eccentric annulus. The eccentricity of the tube is defined as:

$$e = \frac{2E}{d_o - d_i} \dots\dots\dots (\mathbf{IV.1})$$

where E is the offset distance between the center of the inner pipe and the center of the outer pipe, in mm.

The eccentricity of the annular space considered in this work is $\boldsymbol{e = 0.8}$. The inner diameter ID of the annulus is $50\ mm$ and the outer diameter OD is $100\ mm$.

The length of the annulus is 10 m, corresponding to $200\ (r_o - r_i)$, which is sufficient to eliminate the inlet length effect and obtain a fully developed flow within the annulus.

Where r_o and r_i are outer and inner radius of the annulus. A longer annular space $(L = 20m)$ was also simulated and the results were compared with the results for the $10\ m$ annular. The difference between the results for the $10\ m$ and $20\ m$ loops was less than 5%.

In addition, simulations performed by applying a fully developed velocity profile to the inlet boundary yielded results similar to the inlet velocity boundary conditions.

This confirms that the pipe length considered in the current work is long enough to avoid any entrance length effects.

In this study, three oil-based drilling fluids and one water-based drilling fluid were tested. These fluids tested was an industrial fluid already in use in the field.

- **OBMA** is supplied as an oil-based drilling fluid with additional base oil with a density of $1113\ kg/m^3$.
- **OBMB** is an oil-based drilling fluid supplied with base oil but with a density of $1270\ kg/m^3$.
- **OBMC** is **OBMB** with additional organophilic clay added to increase viscosity.

The Herschel-Bulkley model (37) describes non-Newtonian fluid behavior:

$$\tau = \tau_0 + K\dot{\gamma}^n \ldots\ldots\ldots (\text{IV}.1)$$

Here :

- τ(Pa) and τ_y(Pa) are shear stress and yield stress, respectively.
- $\gamma(1/s)$ is shear rate.
- K $(Pa.s)$ and n $(without\ dimension)$ are viscosity consistency index and flow-behavior index, respectively.

The composition of the drilling fluids tested is presented in **Table VI. 1**. The Herschel-Bulkley-model parameters of the drilling fluids are listed in **Table VI. 2.**

Table IV. 1- Composition of OBMA, OBMB, OBMC, and WBM

OBMA	**OBMB**	**OBMC**	**WBM (KCl)**
Base oil EDC 95-11	Base oil EDC 95-11	Base oil EDC 95-11	Fresh water
Barite	Barite	Barite	KCl
Organophilic clay (bentonite)	Organophilic clay (bentonite)	Organophilic clay (bentonite)	Xanthan gum Polynionic cellulose
Salt ($CaCl_2$)	Salt ($CaCl_2$)	Salt ($CaCl_2$)	Glycol
Lime [$Ca(OH)_2$]	Lime [$Ca(OH)_2$]	Lime [$Ca(OH)_2$]	Corn starch
Emulsifier	Emulsifier	Emulsifier	Soda ash
Fluid-loss agent	Fluid-loss agent	Fluid-loss agent Bentonite 128 (organophilic clay)	Barite
$Oil/water$ (ratio 80:20)	$Oil/water$(ratio 80:20)	$Oil/water$(ratio 95:5)	Not applicable

Table IV. 2- Properties of OBMA, OBMB, OBMC, and WBM

Properties	K (Pa.s)	n (-)	$\tau_y\ (Pa)$	Density (Kg/m^3)
OBMA	**0.038828**	**0.88**	**1.6155**	**1113**
OBMB	**(37)**	**0.8759**	**1.73073**	**1270**
OBMC	**0.144892**	**0.8285**	**2.83713**	**1270**
WBM	**1.0362**	**0.42975**	**0**	**1188**

Figure IV.1 and **Figure IV.2** show flow curves of the drilling fluids. Flow curves are measured using an Anton Paar MCR 302 rheometer. **A detailed rheological investigation of tested fluids. (38)**

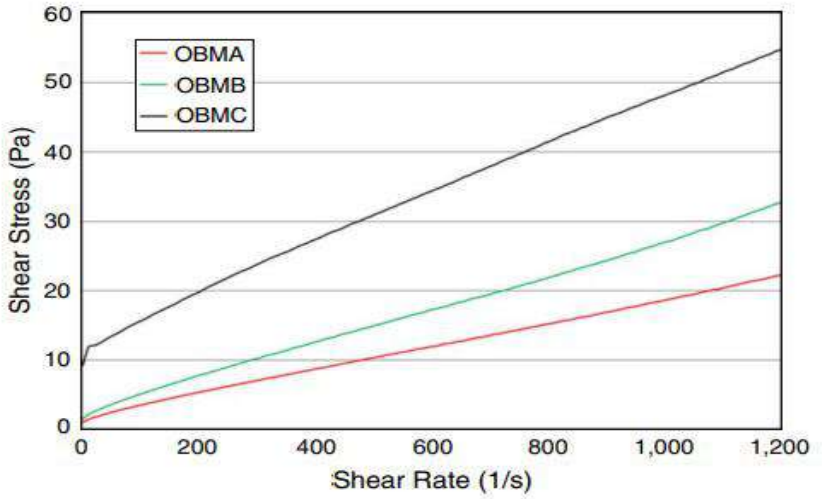

Figure IV. 1- Flow curves of OBMA, OBMB, and OBMC fluids, measurements performed with API RP 13D standard at 28 C°.

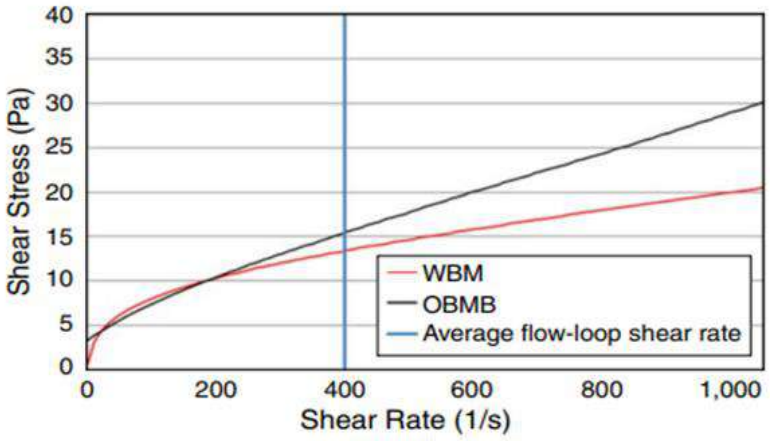

Figure IV. 2- Flow curves of OBMB and WBM fluids, measurements performed with API RP 13D standard at 28 C°

Figure IV. 3- An Anton Paar MCR 302 rheometer

IV.3 Methods

IV.3.1 Experimental Method

IV.3.1.1 Experimental Setup

Experiments to study the hydraulic behavior and well cleaning behavior of different drilling fluids are performed on an advanced purpose-built flow rig. **Figure IV.4** shows a schematic diagram of the test along facility and the circular concrete section used in the test section.

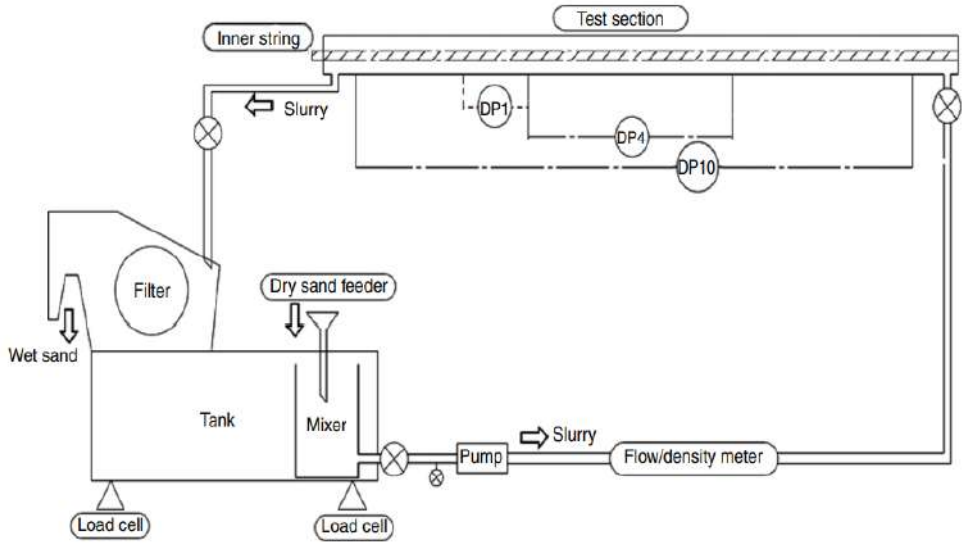

Figure IV. 4-Flow-loop system

The test rig was designed to test and compare hydraulics, cuttings transport and friction for circular and non-circular borehole geometries. The flow system consists of a 10 m long test section, a processing unit (sand injection, sand separation, liquid storage tank and pump), connecting hoses, valves and gauges **(Figure IV.5).**

Figure IV. 5-Purpose-built flow rig.

The 10 m long test track consists of interchangeable concrete hollow cylindrical elements, with an inner diameter of 100 mm representing the drill hole (see **Figure IV. 5**) and a steel rod with a diameter of 50 mm representing the drill string.

One end of the rod is connected to a drive motor to simulate a variable speed system. Both ends of the rod are laterally supported using universal flexible joints, allowing free rotational (lateral) movement within the constraints of the drilled hole.

The movement of the drill string in the axial direction is restricted. Therefore, the drill string is fully eccentric due to the gravity of the drill string. The flow loop is supported by a metal structure that can be tilted 30 degrees from the horizontal.

A transparent cutout was placed in the middle of the test track to visualize the formation of the cutting bed. However, the drilling fluid used in our study was opaque, making visual measurements difficult.

The instrumentation includes a Coriolis flowmeter and two differential pressure (DP) sensors interfaced to the logging system. Monitor flow and density with a Coriolis flowmeter.

The temperature is maintained and continuously monitored by heating elements in the fluid tank.

Differential pressure sensors measure the differential pressure between pressure taps at 3m, 7m and 8m from the inlet, describes a DP unit measurement that measures the pressure difference between ports at 3 m and 7 m positions.

The DP converter was cleaned regularly before each experiment to ensure that the test section was free of air bubbles. Test parameters such as flow, velocity, temperature, density and frictional pressure loss are displayed and recorded by the Labview data acquisition and control system. Calibrate the sand injection system to the preset sand production rate.

The outlet of the test track is connected to a sand separator unit, where liquid and sand are separated. The fluid storage system can hold 5 cubic meters of drilling fluid

(see Figure IV. 6). A load cell below the processing unit is used to measure the change in weight due to the corresponding change in the amount of sand in the test section.

In this way the cuttings holdup in the system could be calculated versus time. The loop is designed for ambient pressure and temperature conditions, which is sufficient for the purposes of our study and is much cheaper than conducting experiments under reservoir conditions.

Figure IV. 6- Fluid storage unit, filtration unit and sand unit

Experimental Procedure

The experimental procedure of the flow loop study is as follows:

✓ **Hydraulic study:**

- The fluid to be measured is circulated in the flow loop circuit by the pump at the desired flow rate.
- Use available pressure transducers for pressure drop measurements under steady state conditions.
- To observe the effect of rotation on pressure drop, the drill string is rotated at the desired rotational speed. The rotational speed is maintained until stable flow conditions are established. Pressure drops measurements at a given drill string rotational speed were made under steady state conditions.
- Repeat test procedure at different flow rates and drill string speeds, and take pressure drop measurements.

✓ **Cuttings transport study:**

• The fluid to be tested is circulated by the pump through the flow loop at a desired flow rate.

IV.3.2 Computational Method

IV.3.2.1 Calculation method

The structured hexahedral computational mesh was generated using the **ANSYS FLUENT 19.2** program. The geometry and computational mesh of the eccentric annulus are shown in **Figure IV. 7**.

A grid independence study was performed using four different mesh size parameters of OBMA, as shown in **Table IV. 3**. The pressure drops obtained in the Grid3 and Grid4 cases are almost equal, and the optimal grid size for the axial, azimuthal and radial directions is 360 × 48 × 12 in this study.

The simulation is assumed to have converged when the residuals error of the continuity and momentum equations reach 10^{-8}. The Reynolds number calculated for the fluids for the experimental test parameters indicates that the flow conditions are in a laminar-flow regime.

The calculated Reynolds number is less than 2500 for all test cases. All simulations were performed in laminar flow regime, which is consistent with the experimental conditions. CFD analysis was performed using ANSYS FLUENT 19.2 software based on the finite volume method. A phase-locked SIMPLE algorithm is used to couple pressure and velocity. Second-order QUICK scheme for discrete momentum and volume fraction equations (ANSYS 2019). At the inlet and outlet of the annulus segment, velocity inlet and outlet boundary conditions are assumed. A non-slip velocity boundary condition that assumes zero fluid velocity at the pipe wall. Flow rates from 0.4 to 1.2 m/s were simulated.

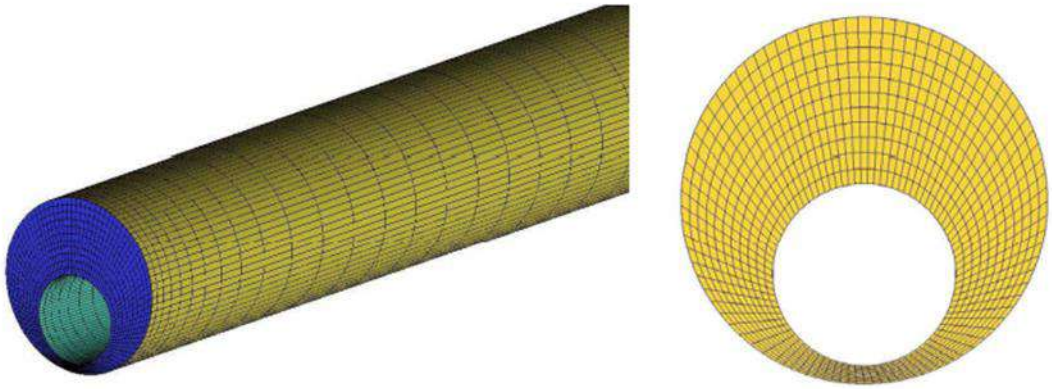

Figure IV. 7- Anulas geometry and computational mesh. Eccentricity

$$e = 0.8; d_i = 50\text{mm}; d_o = 100\text{mm}; L = 10\text{m}$$

Table IV. 3- Grid independence study for OBMA

	Axial	Radial	Azimuthal	Pressure Drop (Pa/m)
Grid1	180	8	24	563
Grid2	240	12	32	542
Grid3	360	12	48	521
Grid4	468	16	48	518

IV.4 Model Validation

The CFD simulation model was validated using experimental data and narrow-slot analysis methods.

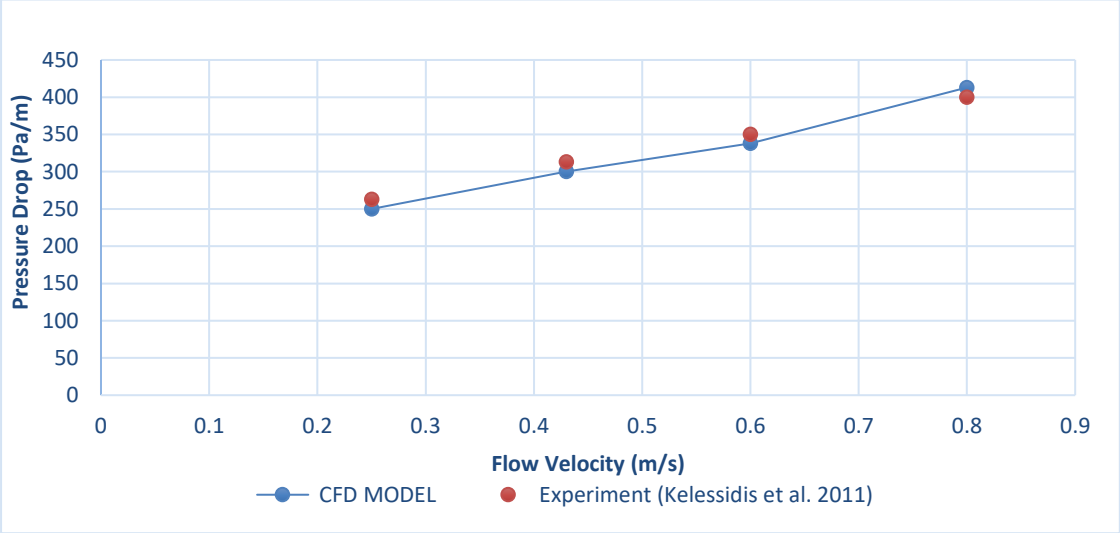

Figure IV. 8-Pressure drop for 1.85% bentonite suspension in water by CFD and experimental results. Herschel Bulkley parameters: $\tau_y = 1.073\ Pa$; $K = 0.0088\ Pa\ s$; $n = 0.8798$. (37)

Figure IV. 8 shows a comparison of the pressure gradient values with the experimental data exist **in** (37).**1. 85**% bentonite suspension in water in $\mathbf{70 \times 40}$ mm concentric annulus.

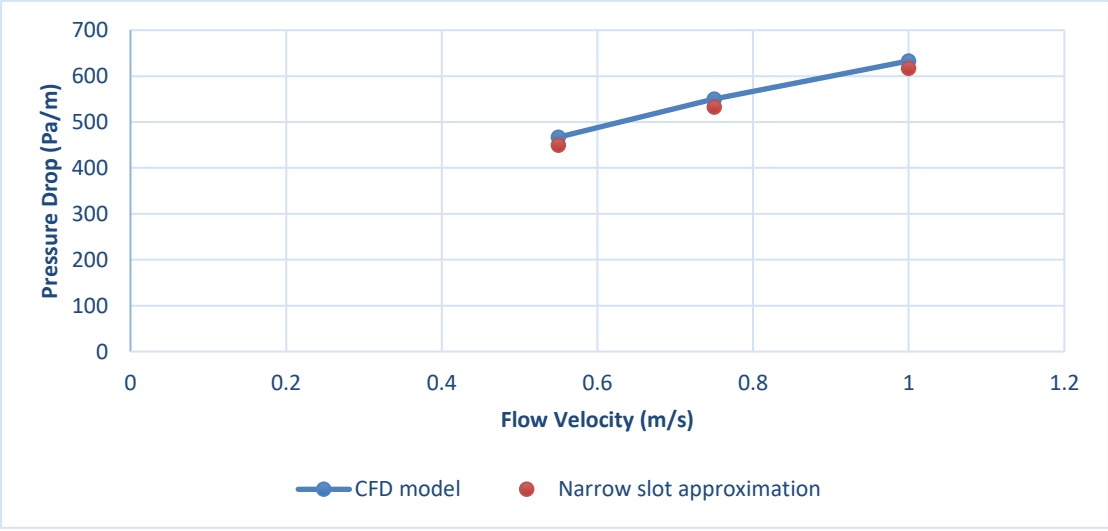

Figure IV. 9- CFD model comparison with narrow-slot approximation for the concentric annulus for OBMA.

Figure IV. 9, the CFD-simulated annular pressure drop of OBMA fluid in concentric annulus is compared with the analytical pressure drop calculated using the narrow-slot approximation method (38). The simulation results are in good agreement with the experimental data, shown in **Figure IV.8**, and the analytical calculations are shown in **Figure IV. 9**, confirming the validity of the CFD model used in the current study.

IV.5 Results and Discussion:

A simulation **without sand injection** into the eccentric annulus is presented. These results are important for analyzing the hydraulic behavior of drilling fluids without particles.

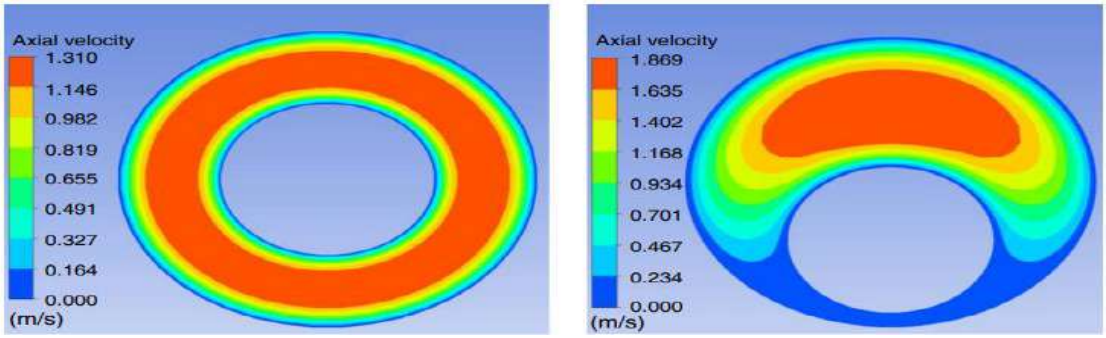

Figure IV. 10- Velocity contour plots for OBMA fluid for average inlet velocity 1 m/s for concentric annulus and eccentric annulus (e=0.8).

The velocity contour plots of the OBMA fluid in concentric and eccentric annular spaces in a plane perpendicular to the flow direction are shown in **Figure IV. 10** for an **average inlet fluid velocity of 1 m/s.**

In the concentric annulus, the velocity distribution is axisymmetric, while in the narrow part of the eccentric annulus, the drilling fluid velocity decreases significantly, while in the wider part, the fluid velocity increases.

As the gap between the inner and outer tubes decreases, the flow resistance increases and the velocity in the narrow part of the annulus decreases. Thus, as

expected, these observations are consistent with earlier results **(this result was reported by (39)).**

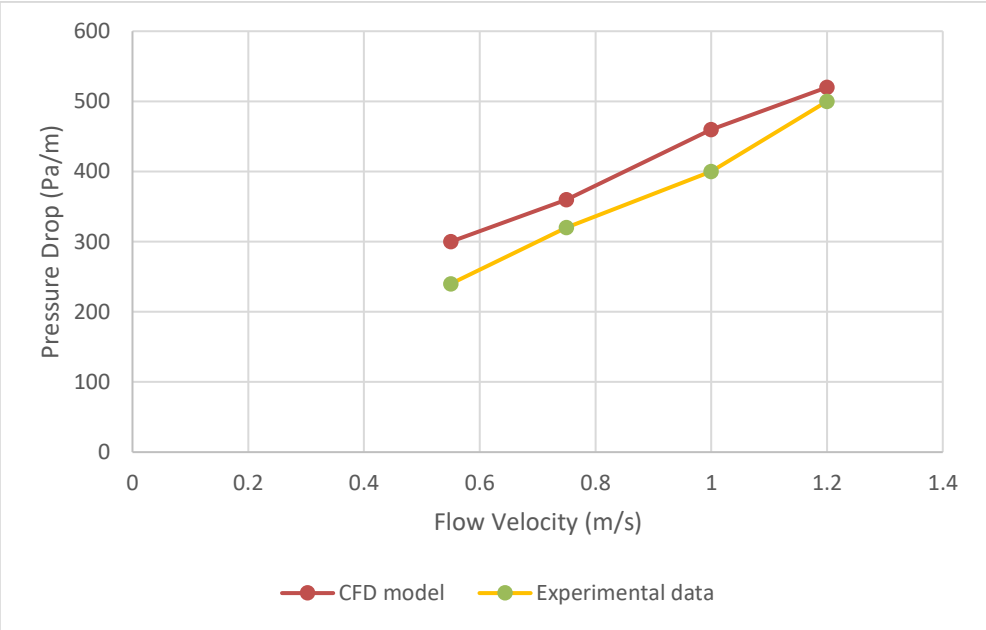

Figure IV. 11- Flow-loop results comparison with CFD-model results for Fluid OBMA at 0 rev/min

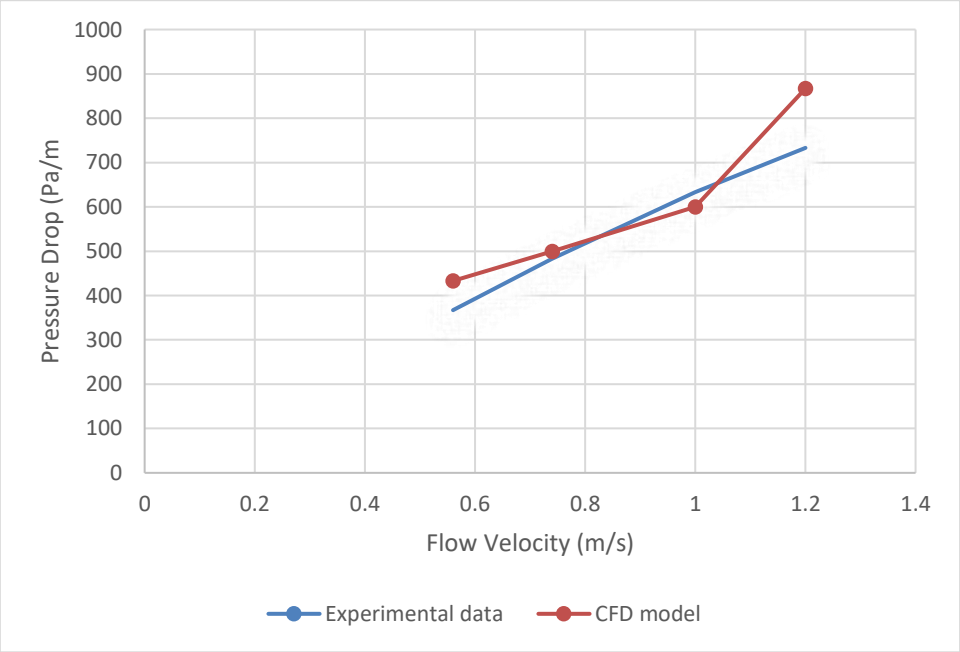

Figure IV. 12-Flow-loop results comparison with CFD-model results for Fluid OBMB at 0 rev/min.

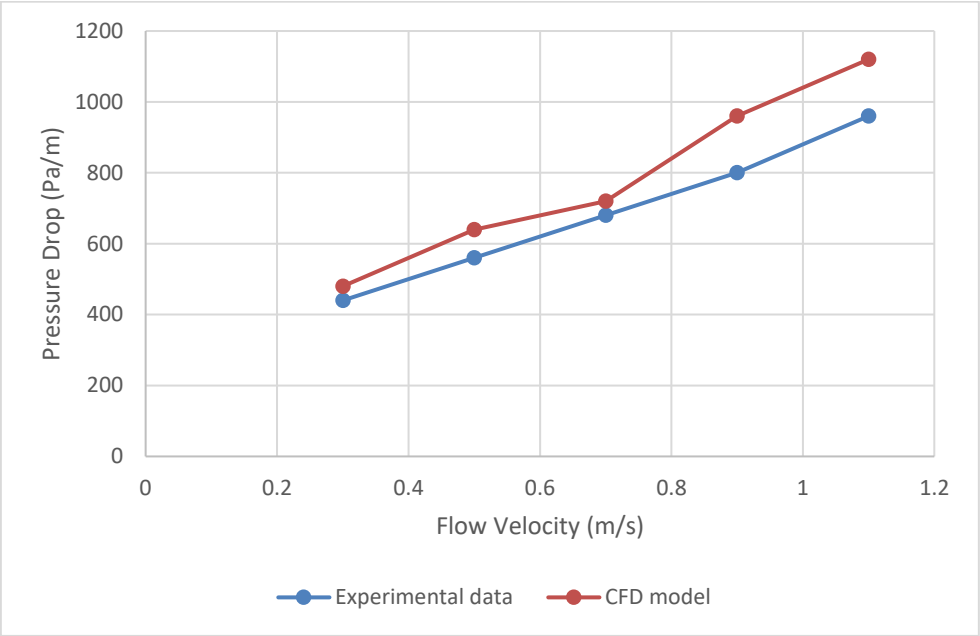

Figure IV. 13- Flow-loop results comparison with CFD-model results for Fluid OBMC at 0 rev/min.

Figures IV. 11-13 show a comparison of pressure drop for a flow loop study using CFD-simulated pressure drop values as a function of increasing fluid velocity for the three OBMs in the eccentric annulus.

For all drilling fluids considered, the pressure drops from the CFD simulations increased with fluid velocity.

The three OBMs tested were liquids with different viscosity and density values. The liquid with the highest viscosity and density, OBMC, had the highest pressure drop of all three liquids, while OBMA, the liquid with the lowest density and viscosity, had the lowest pressure drop of the three liquids.

Furthermore, it can be observed that the reported simulation results agree with the experimental results of the flow loop, with a deviation of less than **15**%.

Numerical simulations were performed for an eccentricity of 0.8, but the experiments were conducted on a fully eccentric annulus. This might result in the small differences observed between the flow-loop and CFD-model pressure drop, as seen in **Figures IV. 11 - IV. 13**.

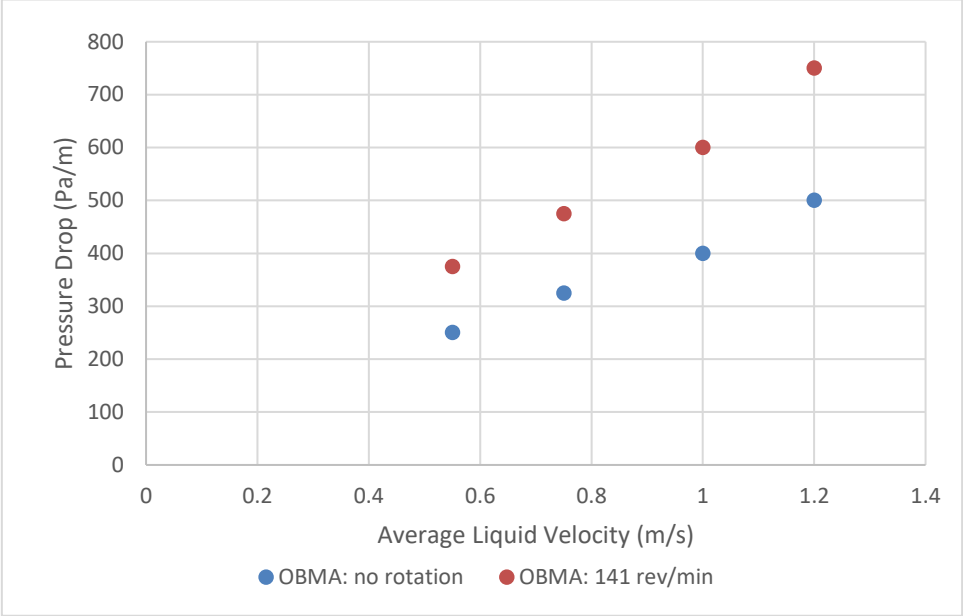

Figure IV. 14- Flow-loop results comparison of Fluids OBMA at 0 rev/min and 150 rev/min.

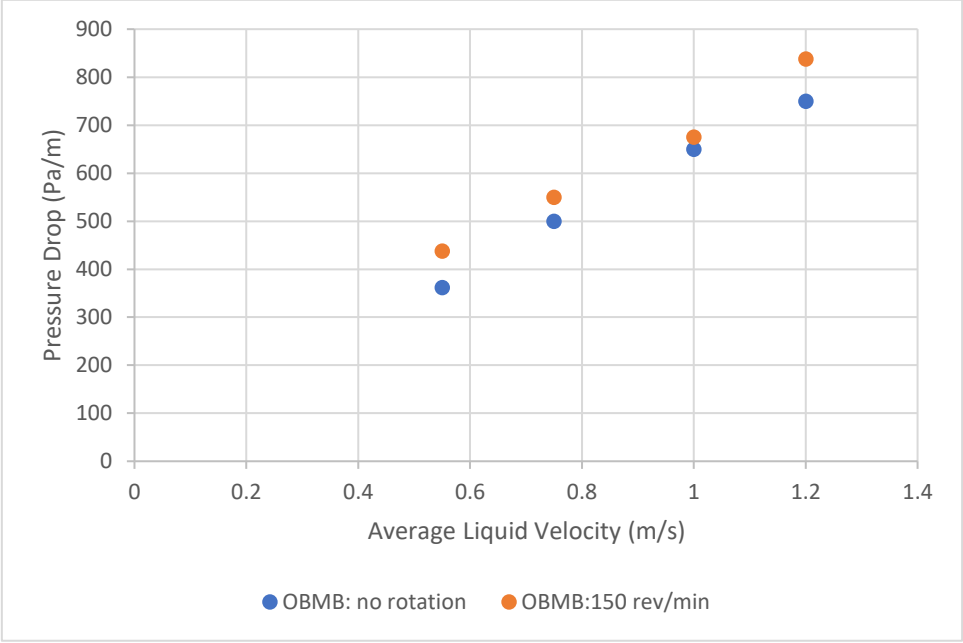

Figure IV. 15- Flow-loop results comparison of Fluids OBMB at 0 rev/min and 150 rev/min.

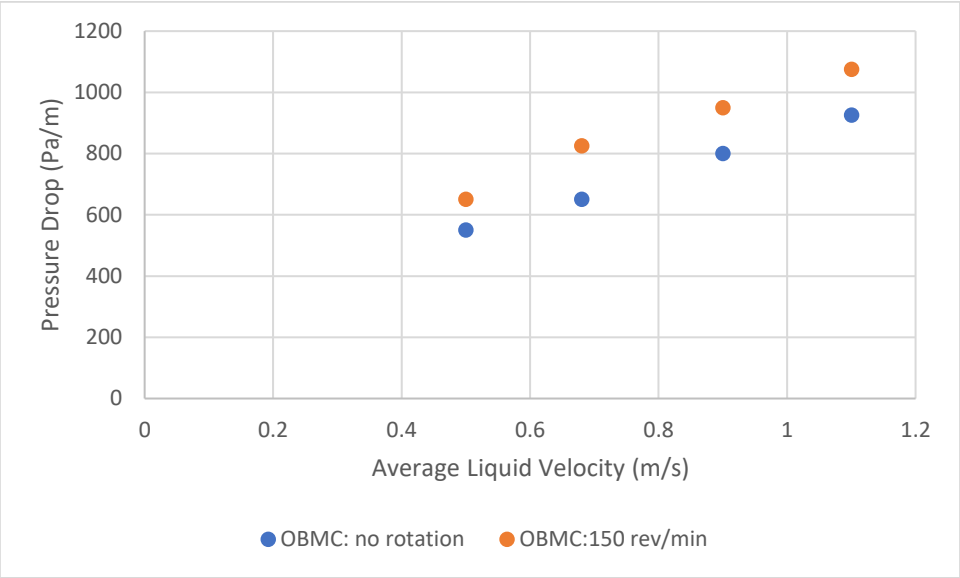

Figure IV. 16- Flow-loop results comparison with CFD model for OBM (OBMC) at 150 rev/min.

Similar behavior was reported from a flow loop investigation, see **Figures IV. 14-16**. Both simulation and experimental results show that the pressure drop increases with fluid velocity.

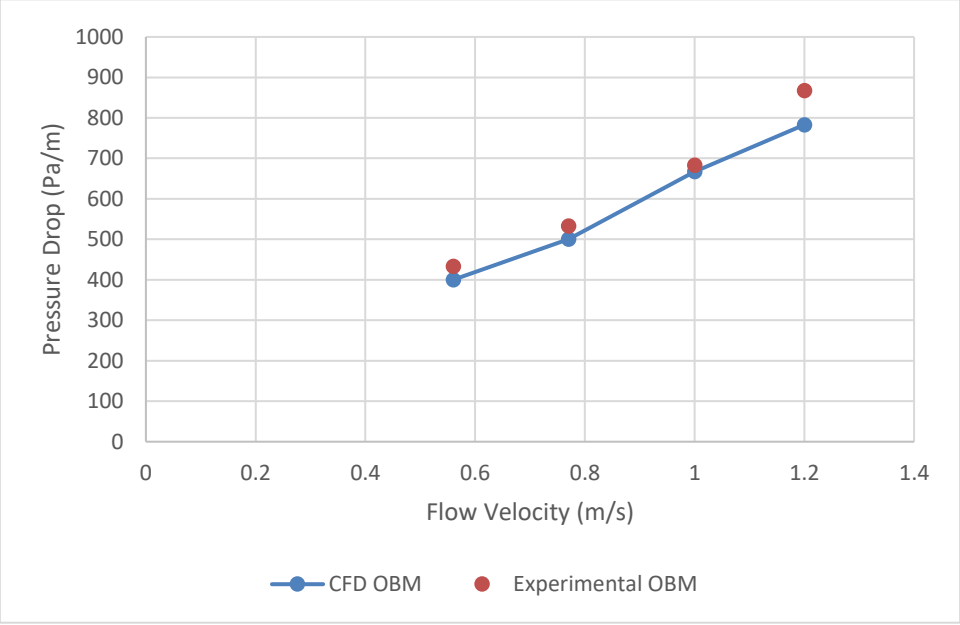

Figure IV. 17-Flow-loop results comparison with CFD model for OBM (OBMB) at 150 rev/min.

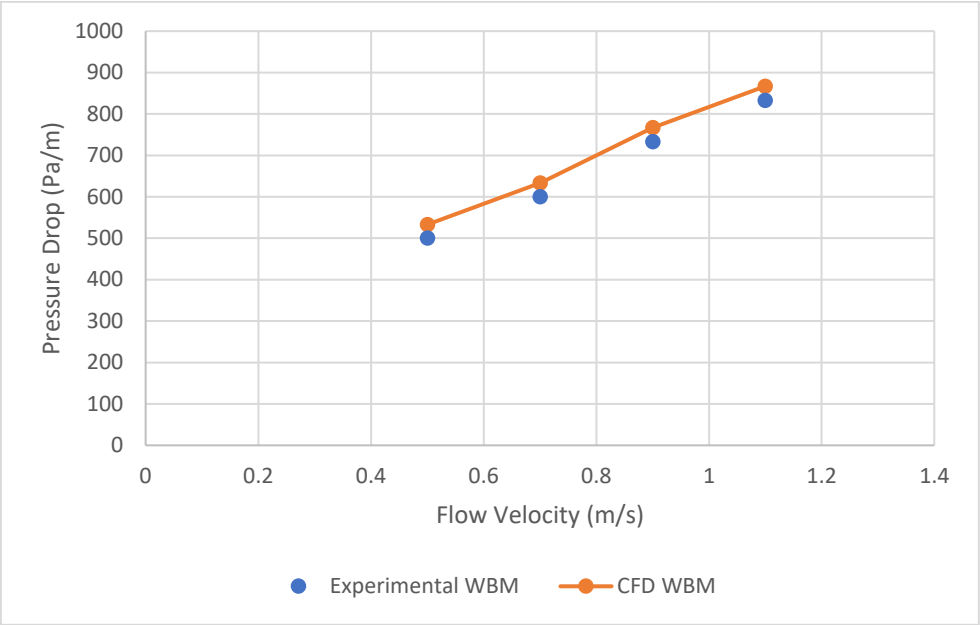

Figure IV. 18-Flow-loop results comparison with CFD model for the WBM at 150 rev/min.

The CFD model has also been extended to incorporate rotation of the drill pipe. In **Figure IV. 17-18**, the pressure drops from CFD simulations of OBMB and WBM at 150 rpm drill pipe rotation is compared with the pressure drop from the flow loop study at 150 rpm.

In the concentric annulus, the rotation of the string reduces the pressure drop in the shear-thinning fluid. As eccentricity increases, inertia becomes more important due to 3D flow effects.

Additionally, during field operations and our flow loop, the string moves laterally, which contributes to inertial effects. Thus, for sufficiently eccentric annulus, the pressure gradient increases with rotation, as inertial effects dominate over shear thinning effects.

For all liquids examined in our study (OBMs and WBM), the shear thinning effect was relatively small. Furthermore, in our experimental setup, the strings are fully eccentric with free lateral motion during rotation, which explains the observed pressure

increase. Compared to similar viscosity curves, the simulation results incorporating drill pipe rotation into the CFD model are in good agreement with the flow loop results.

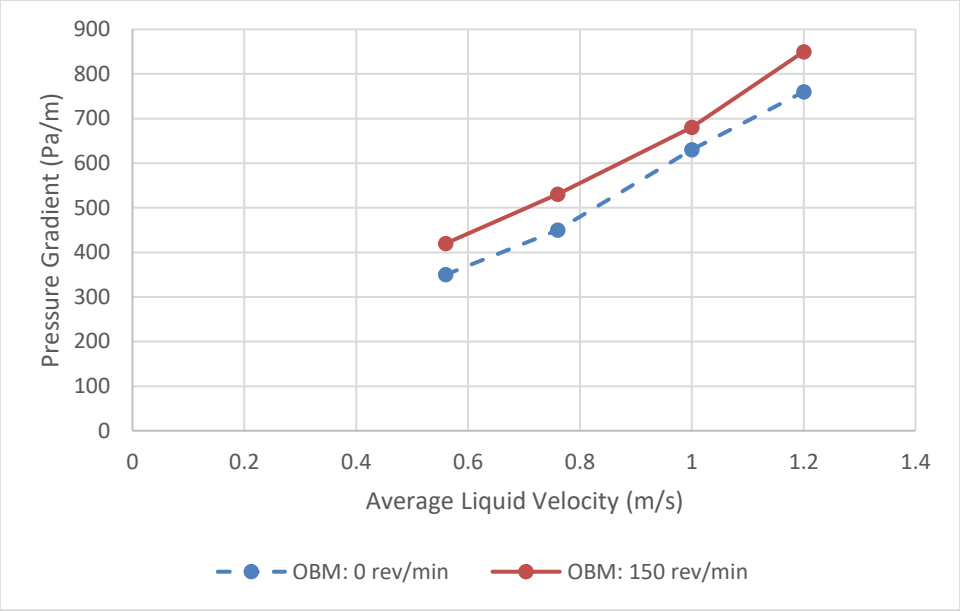

Figure IV. 19- Flow-loop results comparison for OBM (OBMB) at 0 and 150 rev/min

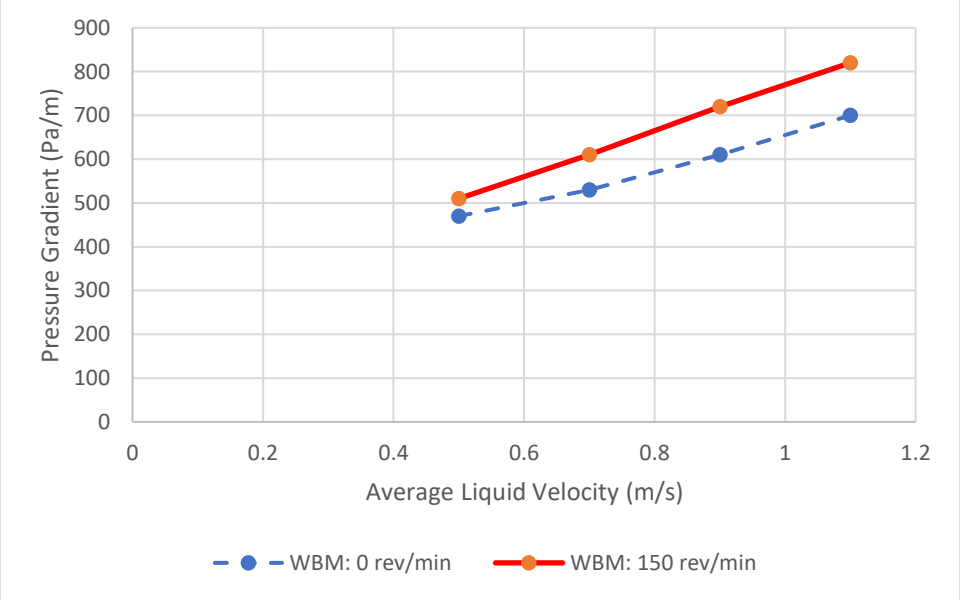

Figure IV. 20- Flow-loop results comparison for WBM at 0 and 150 rev/min.

The pressure gradient value of WBM is higher than that of OBM, although they have almost similar density and viscosity curves, as shown in **Figure IV.19-20**.

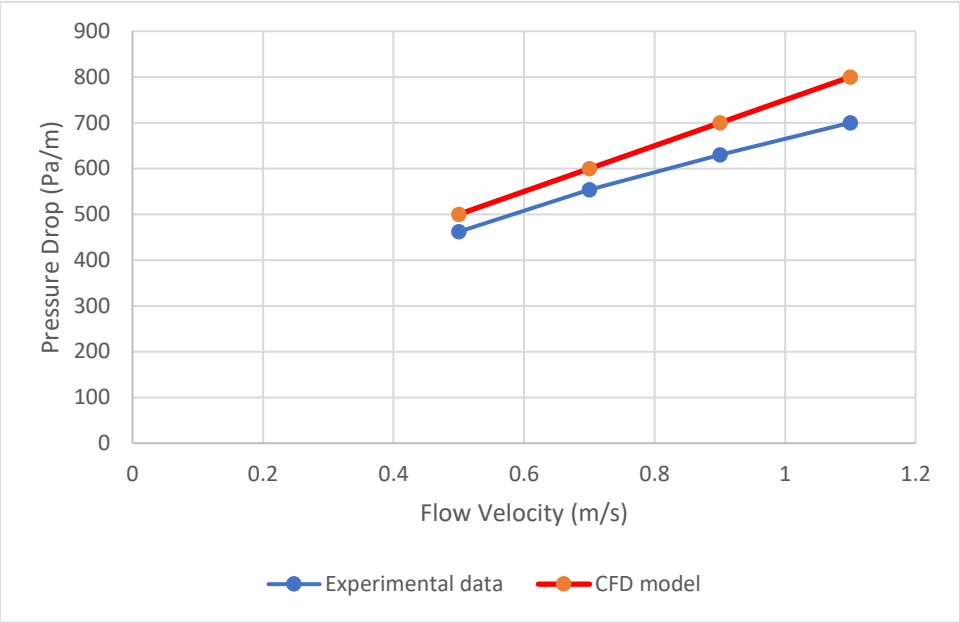

Figure IV. 21- Flow-loop results comparison with CFD-model results for WBM at 0 rev/min.

A comparison of the pressure drop results from the CFD simulation of the WBM with the flow loop results is shown in **Figure IV. 21**.

The CFD simulations of the two fluids (WBM and OBM) agree with the flow loop results. The pressure drops of two liquids with almost similar viscosity profiles are different. As mentioned earlier, the pressure drop increases with the rotation of the eccentric annulus, and the simulation results are consistent with the flow loop results.

These results are consistent with previous theoretical and experimental studies. The WBM has zero yield stress and is modeled in CFD simulations using a power law. The OBM fluid has a specified yield stress and is modeled using the Herschel-Bulkley model.

The main purpose of studying drilling fluids with similar viscosity profiles is to investigate whether their hole cleaning behavior will differ despite similar viscosity profiles.

Based on field experience, OBMs is believed to provide better hole cleaning performance than WBMs (40)**,** while previous laboratory studies have provided conflicting results**.**

A recent study provides flow-loop studies using OBM and WBM with nearly similar viscosity profiles under the same conditions, and shows that OBM provides better hole cleaning performance than WBM without drill string rotation.

Additionally, the hole cleaning performance of OBM and WBM is nearly identical to existing drill string rotation.

In the absence of drill string rotation, the sand holdup of WBM is significantly higher than that of OBM. In the presence of drill string rotation, the sand retention behavior of WBM and OBM is likely to be the same.

In our study, sand holdup was used to compare the hole cleaning performance of drilling fluids. Sand bed hold-up was defined as the average amount of sand remaining on the test track at the end of the test. These experimental studies, combined with CFD simulations, can be used to build better and more accurate models of cuttings transport.

IV.6 Conclusions

The developed CFD model is validated with previous studies and performed flow loop experiment in the annular flow velocity range of 0.4 to 1.0 m/s.

The present numerical study investigates the frictional pressure loss of different non-Newtonian drilling fluids in concentric and eccentric horizontal annular space under laminar flow regime without cuttings particles.

• The developed CFD model is in good agreement with the results of the flow loop study.

• Increasing annular fluid velocity significantly increases frictional pressure loss. Low-density, and low-viscosity drilling fluids have lower pressure drops, while high-density, and high-viscosity drilling fluids have higher pressure drops.

• Frictional pressure losses are different for drilling fluids with similar viscosity profiles, which have been observed in experiments and CFD simulations. OBM and WBM with similar viscosity profiles were tested. Although the viscosity curves are similar, the frictional pressure drop of OBM and WBM is different. The hole cleaning behavior of OBM and WBM is also different. With absence rotation of the drill string, hole cleaning with OBM was significantly better than with WBM. At high drill string rotation, the hole cleaning performance of WBM is close to that of OBM.

• A significant increase in pressure drop was observed as the drill string was rotated. The competing effects of inertia and shear thinning cause the pressure drop in the eccentric annulus to increase as the drill string rotates.

• Developed models can be used for further studies with different liquids, saving time and money. By including particles in the simulation, the developed model can be further extended to study the transport behavior of drill cuttings by different drilling fluids. Evaluating the hydraulic and hole-cleaning behavior of fluids under the same conditions facilitates the development of more accurate models for estimating the hydraulic and hole-cleaning efficiency of drilling fluids.

In this study, CFD simulations were performed with various OBMs and WBMs without cuttings. When cuttings are applied, the conditions become more complex and it might be more difficult to discover errors.

The case without cuttings is the simplest, and this must match the corresponding experiments before running more-complex and more-time-consuming cases.

V. General conclusions & recommendations:

Drilling fluid is used to rise the cuttings made by the bit and lift them to the surface for disposal. But equally important, it also provides a means of keeping underground pressures in check.

Rheological models used in describing the rheology of non-Newtonian fluids include but not limited to the following: The Bingham Plastic Model, the Power Law Model, Herschel-Bulkley Model. Selection of the best rheological model that accurately represents the shear stress-shear rate analysis is to achieving correct results for pressure drops and hydraulic calculation.

The finite volume method usually yields systems of equations. Since the systems arising from realistic CFD problems can be very large – up to 100 000 to 1 million equations – we find that iterative methods are generally much more economical than direct methods.

The complexity and size of the set of equations depends on the dimensionality of the problem, the number of grid nodes and the discretization practice. Although any valid procedure can be used to solve the algebraic equations, the available computer resources set a powerful constraint.

The present numerical study investigates the frictional pressure loss of different non-Newtonian drilling fluids in concentric and eccentric horizontal annular space under laminar flow regime without cuttings particles.

The developed CFD model is in good agreement with the results of the flow loop study.

- Increasing annular fluid velocity significantly increases frictional pressure loss.
- Low-density, and low-viscosity drilling fluids have lower pressure drops and vice versa.

- Frictional pressure losses are different for drilling fluids with similar viscosity profiles, , the frictional pressure drop of OBM and WBM is different. The hole cleaning behavior of OBM and WBM is also different.
- With absence rotation of the drill string, hole cleaning with OBM was significantly better than with WBM.
- At high drill string rotation, the hole cleaning performance of WBM is close to that of OBM.

VI. References:

1. **Dhiman, Annudeep Singh.** *Rheological properties & corrosion characteristics of drilling mud additives.* s.l. : Submitted in partial fulfillment of the requirement for the degree of Master of Engineering, Dalhousie University Halifax, Nova Scotia, September 2012.

2. **AKILIMALI, FORTUNE CHRISTIAN.** *laboratory practical on analysis of the factors that affects the properties of the drilling mud during drilling process.* s.l. : the university of dodoma, college of earth science school of mines and petroleum engineering, department of petroleum and energy engineering, 15th July 2016.

3. ***Drilling Fluids Manual.*** **s.l. : Amoco Production Company.**

4. ***IADC Drilling Manual eBook Version (V.11).*** **s.l. : International Association of Drilling Contractors All Rights Reserved, 2000.**

5. Ali, Mr. BENAÏSSA. ***Performance Evaluation of HP WBM Drilling Fluid in Hassi Messaoud Field from the 16" Hole Section.*** **s.l. : Professional Project in Partial Fulfillment of the Requirements For the degree of Specialized Magister in Drilling & Production Engineering, Algerian petroleum institute, Boumerdes School, December2014.**

6. OSOKOGWU, Uche, AJIENKA, Joseph Atubokiki et OKON, Andrew Nsika. ***Evaluating the Effects of Additives on Drilling Fluid Characteristics.*** **Nigeria : International journal of engineering sciences & research technology, Department of Petroleum and Gas Engineering, University of Port Harcourt, P M B 5323, Choba, Port Harcourt, Rivers State, June 2014.**

7. ***Siderite as a weighting material in drilling mud.*** **Abou Alfa, Khaled, Harkouss, Rami and Khatib, Jamal. December 2019, BAU Journal - Science and Technology: Vol. 1,Iss. 1 , Article 1, p. https://digitalcommons.bau.edu.lb/stjournal/vol1/iss1/1.**

8. HEZRON, SIMON. ***Laboratory practical on analysis of the factors that affects the properties of the drilling mud during drilling process.*** **s.l. : The university of**

dodoma, college of earth sciences,school of mines and petroleum engineering,department of petroleum and energy engineering, 14th JUNE 2017.

9. Khodja, Mohamed, et al. ***Drilling Fluid Technology: Performances and Environmental Considerations.*** **s.l. : Products and Services; from R&D to Final Solutions.**

10. LYONS, WILLIAM C. ***Working guide to drilling equipment and operations.*** **s.l. : Published by Elsevier Inc. All rights reserved, 2010.**

11. ALJADI, RAMZI. ***Drilling fluids technology, DRILLING FULIDS ENGINEER #2.***

12. ***Drilling Fluid Engineering.*** **Skalle, P,. 2010, APS, Trondheim,.**

13. ***A generalized model for apparent viscosity of oil-based muds.*** **Muili F. Fakoya, Ramadan M. Ahmed. 5 March 2018, Journal of Petroleum Science and Engineering.**

14. ***Frictional pressure loss of drilling fluids in a fully eccentric annulus.*** **Oney Erge, Ali Karimi Vajargah, Mehmet Evren Ozbayoglu, Eric van Oort. 18 July 2015, Journal of Natural Gas Science and Engineering.**

15. ***Nanoparticles on the Rheological Properties of Water Based Mud Under HighPressure and temperature Environment.*** **Anawe P.A.L and Folayan, J.A. 2018, International Journal of Mechanical Engineering.**

16. Paul Anawe, Adewale Folayan. ***Advences in Drilling Fluids Rheology.*** **· January 2019.**

17. HALLIBURTON. ***Baroid Fluids Handbook.*** **s.l. : Engineering , 2012.**

18. understanding yield point; effect on pressure surges critical to managing deep difficult MPD wells. ***www.DRILLING CONTRACTOR.org.*** **[En ligne] 3 nov 2009.**

19. types of flow and rheology models of drilling mud. ***www.drilling formulas.com.*** **[En ligne]**

20. Isayev, Prof. Dr. Alexander Ya. Malkin. Prof. Dr. Avraam. ***Rheology Concept, Methods, and Applications 3rd Edition.*** **toronto : s.n., 2017.**

21. Amoco Production Company. ***Rheology, Hydraulics, and Hole Cleaning.***

22. ***Weir, I.S., Bailey, W.J. A statistical study of rheological models for drilling fluids.*** **BAKER HUGHES. s.l. : SPE, 1996.**

23. ***Rheological Characteristics of Oil-Based and Water-Based Drilling Fluids.*** **Mahmoud Khalifeh1*, Arild Saasen1 and Karl Ronny Klungtvedt1,2. August 2021.**

24. Guria., Chandan. ***Rheological analysis of drilling fluid using Marsh Funnel .*** **India. : Department of Petroleum Engineering, Indian School of Mines, Dhanbad 826004, , (2013).**

25. Maglione, R., Robotti, G., Romagnoli, R.,. ***In-situ rheological characterization of drilling mud. SPE J. 5, 377–386.*** **2000.**

26. ***Reiner, M. (1926). KolloidZ39,80-87.***

27. Bingham, E.C. (1922). Fluidity and plasticity. MC Graw-hill, New York.

28. ***American Petroleum Institute . Recommended Practice on the Rheology and Hydraulics of Oil-Well Drilling fluids API RP13D.*** **s.l. : American Petroleum Institute , 1995.**

29. MARK S. RAMSEY, P. E. ***PRACTICAL WELLBORE HYDRAULICS AND HOLE CLEANING Unlock Faster, More Efficient, and Trouble-Free Drilling Operations.*** **USA : Elsevier, 2019.**

30. Alexandre Lavrov SINTEF Petroleum Research, Trondheim, Norway. ***Lost Circulation Mechanisms and Solutions.*** **NORWAY : ELSEVIER, 2016.**

31. ***The Effects of Fluid Rheology and Drillstring Eccentricity on Drilling Hydraulics.*** **Anthony Kerunwa, Julian Ubanozie Obibuike, Ugochukwu Ilozurike Duru. Nigeria : s.n.**

32. Darwish, M. ***The Finite volume method in CFD An Advanced Introduction.*** **[éd.] Spinger.**

33. V.Patankar, Suhas. ***Numerical heat transfer and fluid flow.***

34. Malalasekera, H K Versteeg and W. ***An Introduction to computional fluid dynamics , the finite volume method second edition.***

35. John D. Anderson, Jr. ***COMPUTATIONAL FLUID the basics with applications.***

36. Sayindla, Sneha. Study of Cuttings Transport Using. ***Study of Cuttings Transport Using.*** **2018.**

37. ***Experimental study and predictions of pressure losses of fluids modeled as Herschel–Bulkley in concentric and eccentric annuli in laminar, transitional and turbulent flow.*** **Kelessidis, Vassilios C.**

38. ***Laminar, Transitional and Turbulent Flow of Herschel–Bulkley Fluids in Concentric Annulus.*** **Founargiotakis, K.**

39. ***Non-Newtonian Flow in Eccentric annuli.*** **Haciislamoglu, M.**

40. ***Hole Cleaning During Deviated Drilling - The Effects of Pump Rate and Rheology.*** **Saasen, A.**

41. ***Novel equation for the prediction of rheological parameters of drilling fluids in an annulus. Industrial and Engineering Chemistry.*** **Nasiri, M., & Ashrafizadeh, S. N. (2010).**

42. Bertram, Volker. ***Practical Ship Hydrodynamics.*** **s.l. : Elsevier, 2012.**

43. ***Finite Volume Methods.*** **al, Robert Eymard et. s.l. : Elsevier, pp. .713-1020.**

44. Jasak, Hrvoje. Error Analysis and Estimation for finite volum method ith application to fluid flow. 1996.